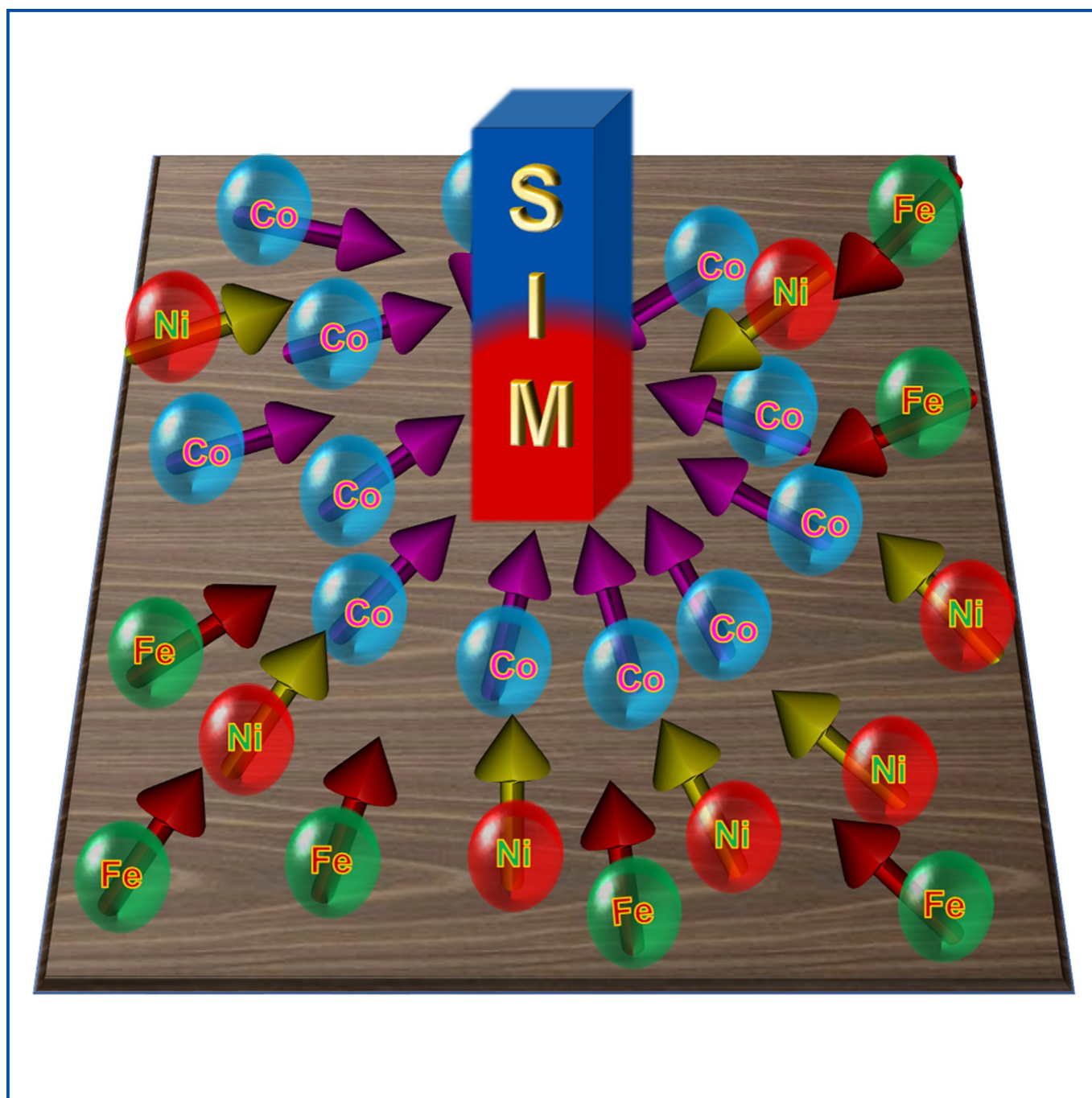


■ Single-Ion Magnets

Role of Coordination Number and Geometry in Controlling the Magnetic Anisotropy in Fe^{II}, Co^{II}, and Ni^{II} Single-Ion MagnetsArup Sarkar, Sourav Dey, and Gopalan Rajaraman*^[a]

Abstract: Since the last decade, the focus in the area of single-molecule magnets (SMMs) has been shifting constructively towards the development of single-ion magnets (SIMs) based on transition metals and lanthanides. Although ground-breaking results have been witnessed for Dy^{III}-based SIMs, significant results have also been obtained for some mononuclear transition metal SIMs. Among others, studies based on Co^{II} ion are very prominent as they often exhibit high magnetic anisotropy or zero-field splitting parameters and offer a large barrier height for magnetisation reversal. Although Co^{II} possibly holds the record for having the largest number of zero-field SIMs known for any transition metal ion, controlling the magnetic anisotropy in these systems

are still a challenge. In addition to the modern spectroscopic techniques, theoretical studies, especially *ab initio* CASSCF/NEVPT2 approaches, have been used to uncover the electronic structure of various Co^{II} SIMs. In this article, with some selected examples, the aim is to showcase how varying the coordination number from two to eight, and the geometry around the Co^{II} centre alters the magnetic anisotropy. This offers some design principles for the experimentalists to target new generation SIMs based on the Co^{II} ion. Additionally, some important Fe^{II}/Fe^{III} and Ni^{II} complexes exhibiting large magnetic anisotropy and SIM properties are also discussed.

Introduction


To achieve the goal of miniaturisation of electronic devices, the scientific community has come its closest in recent years to creating the smallest quantum storage devices in the form of molecular nanomagnets and quantum logic gates, etc.^[1] To utilise molecular magnets for the potential applications proposed, it is important to keep the temperature at which the magnetisation is fully frozen (blocking temperature T_B) as high as possible. The development in the area of single-molecule magnets (SMMs) has undergone revolutionary progress recently, as the blocking temperature (T_B) of [Dy(Cp^{ttt})₂]⁺ and [(Cp^{ipr5})Dy(Cp^{*})]⁺ lanthanide complexes reached 60 K and 80 K, respectively, taking the T_B beyond liquid nitrogen temperatures.^[2] The ultimate goal for the scientific community is to anchor these molecules on surfaces such that it can retain the magnetic properties and fabricate molecule-based memory storage devices. Such devices upon fabrication are expected to store information at 30 TB cm⁻² capacity and this is significantly higher than the current industry standards.^[2a,3] Although lanthanide-based molecules are of great interest as they exhibit fascinating magnetic properties compared with its peers, the abundance of the lanthanide elements, particularly Dy, is minuscule in the earth's crust (5.2 mg kg⁻¹) and are found only in selected geographical locations.

Transition-metal complexes offer a viable alternative to the lanthanides, and several recent reports on earth-abundant first-row transition metal ion-based single-ion magnets offer tantalising possibilities to utilise them for the potential applications proposed. In this regard, low-coordinate transition-metal complexes such as [(NHC)CoNDmp] and [Co(C(SiMe₂ONaph)₃)₂] are promising as these show very strong magnetic coercivity with effective magnetisation reversal barriers (U_{eff}) of 413 cm⁻¹ and 450 cm⁻¹, respectively.^[4] Although lanthanide chemistry is

relatively well developed at present, single-ion magnets based on transition metal ions are at a nascent stage and face significant challenges such as air stability, under barrier relaxation of magnetisation, fast quantum tunnelling of magnetisation (QTM), relaxation of magnetisation via other mechanisms such as phonon bottle-neck, etc. These challenges necessitate deep theoretical understanding and a design principle for transition metal ion based mononuclear SMMs or single-ion magnets (SIMs).^[1b] Particularly, controlling the magnetic anisotropy in SIMs is crucial, and this is correlated to the splitting of the ground state spin manifold in the absence of a magnetic field (called zero-field splitting). It is understood that the above-mentioned characteristics depend upon various factors such as (i) spin-orbit coupling (SOC) of the metal ion, (ii) shape of the metal electron density at the ground state, (iii) surrounding ligand environment and symmetry, (iv) orbital orderings and degeneracy, (v) intermolecular and intramolecular exchange interactions, and (vi) nuclearity of metal-ligand clusters, etc.

Several experimental and theoretical investigations have revealed that mononuclear lanthanide (Ln), as well as transition metal (TM) complexes, are superior to polynuclear systems in obtaining very large U_{eff} values.^[5] Polynuclear complexes often suffer faster magnetisation relaxation owing to weak intramolecular exchange coupling and smaller ZFS (zero-field splitting) parameters, which tend to decrease with the increase in S value.^[6] Various magnetic measurement techniques such as direct current (dc) susceptibility and magnetisation studies, alternating current (ac) susceptibility methods are often used method to assess the nature of anisotropy. However, accurate information about the ZFS parameter can be obtained from techniques such as high-field high-frequency EPR, variable field THz spectroscopy, far-IR spectroscopy, torque magnetometry, NMR paramagnetic shift, and INS (inelastic neutron scattering) studies. As these studies are scarce, the ZFS parameters are generally obtained by fitting the temperature-dependent susceptibility and low-temperature magnetisation data. These experimental data are often insensitive to the sign of the D value, and at many times also the magnitude, and hence is not a reliable tool to accurately estimate the ZFS parameters.^[7] Particularly for molecules possessing a ZFS parameter larger than

[a] A. Sarkar, S. Dey, Prof. G. Rajaraman
Department of Chemistry, Indian Institute of Technology Bombay
Mumbai 400076 (India)
E-mail: rajaraman@chem.iitb.ac.in

 The ORCID identification number(s) for the author(s) of this article can be found under: <https://doi.org/10.1002/chem.202003211>.

100 cm^{-1} , it is often difficult to establish both sign and magnitude as there are only a handful of laboratories around the world that have access to facilities that can precisely characterise such strongly anisotropic systems.^[7–8]

Theoretical Background

Theoretical tools based on wavefunction techniques such as SA-CASSCF (state-averaged complete active space self-consistent field) methods are becoming increasingly indispensable as they not only offer a reliable estimate of the sign/magnitude of these parameters but also offer insight into the origin of such strong anisotropy and thus provide the much-needed design principle to obtain superior SIMs. In probing the origin of magnetic anisotropy, post-Hartree–Fock multi-reference calculations such as CASSCF/NEVPT2 (N-electron valence perturbation theory second-order)/CASPT2 (complete active space second-order perturbation)/MRCI (multi-reference configuration interaction)/DMRG (density matrix renormalisation group) are found to be superior to that of the DFT (density functional theory) techniques. Often large anisotropy arises from orbital degeneracy of the ground state, and this cannot be handled by the single determinant method such as DFT.^[9] Neese et al. investigated the origin of magnetic anisotropy and Spin-Hamiltonian parameters in mononuclear systems initially through semi-empirical and DFT methods. Later, the group proposed very accurate post-Hartree–Fock multi-configuration approaches.^[10] Also, the modern universal technique of estimation of ZFS (zero-field splitting) parameters, that is, the Effective Hamiltonian Approach (EHA) was developed by Guihéry and co-workers way back in 2009.^[11] These theoretical methods have been gaining ground over the years and are a reliable tool to estimate the ZFS parameters; they have now reached a level wherein they can be utilised to offer a prediction on molecules that are not magnetically characterised or yet to be synthesised.^[12] In this short review, we aim to explore the recent examples in this area wherein both experiments and theory are utilised side-by-side to uncover the origin of large anisotropy in transition metal SIMs.

Zero-Field Splitting in Transition Metal-Based SIMs

Although the research in TM-based SMMs began with the archetypal Mn_{12} cluster, soon, it was realised that mononuclear complexes offer stronger magnetic anisotropy.^[6a,b] It is well-known that the U_{eff} for TM systems is proportional to the product of axial zero-field splitting parameter D times the square of the z-projection of total spin, that is, S_z^2 assuming transverse anisotropy is negligible. The original phenomenological ZFS Hamiltonian is given by [Eq. (1)]:

$$\hat{H} = \hat{S} \cdot \mathbf{D} \cdot \hat{S} \quad (1)$$

where D is a second rank tensor and S is the resultant spin ground state. After diagonalizing the D tensor and making D traceless, that is, $D_{xx} + D_{yy} + D_{zz} = 0$, there are two ZFS param-

eters introduced, namely the axial ZFS parameter D and rhombic parameter E [Eq. (2)]:

$$D = D_{zz} - \frac{1}{2}(D_{xx} + D_{yy}); E = \frac{1}{2}(D_{xx} - D_{yy}) \quad (2)$$

Thus, the complete ZFS Spin-Hamiltonian is given by the following equation^[11,13] [Eq. (3)]:

$$\hat{H}_{\text{ZFS}} = D \left[\hat{S}_z^2 - \frac{1}{3}S(S+1) \right] + E(\hat{S}_x^2 - \hat{S}_y^2) \quad (3)$$

where D and E are the axial and rhombic ZFS parameters, respectively, and S , S_x , S_y , and S_z represent the total spin and its corresponding x , y , and z components, respectively. The components of the D parameter are theoretically determined by

Gopalan Rajaraman received his PhD at the University of Manchester, UK. Later, he moved to the University of Heidelberg, Germany, as AvH post-doctoral fellow and then moved to the University of Florence, Italy, for a second post-doctoral stint with a Marie-Curie IIF fellowship. In December 2009, he joined IIT Bombay, India, as an assistant professor and became a professor in 2018. His research focuses on employing electronic structure methods to understand the structure, properties and reactivity of molecules possessing unpaired electrons (open-shell systems). In addition to modelling molecular magnets, his group also actively pursues research in the area of modelling biomimetic reactions catalysed by high-valent metal-oxo/imido complexes.



*Arup Sarkar completed his Bachelor's degree in Chemistry at Seth Anandram Jaipuria College, University of Calcutta, Kolkata, in 2012. He finished his Master's degree with specialization in Inorganic Chemistry at the University of Calcutta (Rajabazar Science College, Kolkata) in 2014. He then moved to the Indian Institute of Technology Bombay, Mumbai in 2015 to conduct his Ph.D. research under Prof. Gopalan Rajaraman at the Department of Chemistry. He is currently a CSIR-SRF fellow, and his major research interests include investigation of magnetic anisotropy in single-ion magnets containing transition metal and lanthanide ions through *ab initio* and DFT methodologies.*



*Sourav Dey completed his Bachelor's degree in Chemistry at Ramakrishna Mission Vidya-mandira, Howrah in 2014. He obtained his master's degree with specialization in computational chemistry from IIT Kharagpur, West Bengal in 2016. He moved to IIT Bombay, Mumbai in 2016 to conduct his Ph.D. research under supervision of Prof. Gopalan Rajaraman. He is currently a UGC-SRF fellow and his research interests cover the investigation of magnetic anisotropy in lanthanide and actinide-based complexes using DFT and *ab initio* techniques.*



the second-order perturbation approach and has a negative sign from the following relation [Eq. (4)]:

$$D_{ij} = -\frac{\zeta^2}{4S^2} \sum_{p,q} \frac{\langle \Psi_p | \hat{l}_i | \Psi_q \rangle \langle \Psi_q | \hat{l}_j | \Psi_p \rangle}{\varepsilon_q - \varepsilon_p} \quad (4)$$

where i and j are the components (x or y or z) of the D tensor, ζ is the effective spin-orbit coupling constant of the metal ion, Ψ_p , Ψ_q , ε_p , ε_q are the ground state (denoted as index p) and excited state (denoted as index q) wavefunction and their respective energies, and \hat{l}_i and \hat{l}_j are the x , y , and z components of the angular momentum operator. Equation (4) is valid only for transition between same spin multiplicity while spin flip contribution towards D has additional terms. The wavefunctions are in fact multi-configurational in nature and hence cannot be described by a single determinant formula. In CASSCF type calculations, normally, a minimal active space of CAS(n , m) is chosen (where n is the number of 3d electrons and m is the number of 3d orbitals, which is 5) to calculate all the ligand field (d - d transitions) excited state energies. Expansion of these active space and inclusion of bonding ligand orbitals or vacant virtual metal-based orbitals are also sometimes necessary for strong covalent bonding situations. Further treatment of dynamic correlations like CASPT2 or NEVPT2 on the top of the CASSCF wavefunction almost accurately reproduces the ligand field energies, and after perturbative treatment of spin-orbit coupling (QDPT) this method reproduces the Spin-Hamiltonian parameters quit well.

From equations (2) and (4), it is clear that D becomes negative when D_{zz} overcomes the $\frac{1}{2}(D_{xx} + D_{yy})$ term. It is necessary to remember that equation (4) is valid for spin-allowed electronic transitions only. Equation (4) also explains that spin-allowed same M_L valued transitions to contribute to the negative D , whereas different M_L valued transitions contribute to the positive D values. Rhombic ZFS parameter E (or E/D) corresponds to the difference in the transverse components of D , that is, $D_{xx} - D_{yy}$.

Now let us briefly explain the ZFS in terms of the splitting of the Kramers pairs in the Co^{II} ion. Using equation (3), one can easily find the eigenvalues of the Kramers pairs, that is, M_S levels like in Figure 1. When D is positive, the $|\pm 1/2\rangle$ state stabilises and when D is negative, $|\pm 3/2\rangle$ is stabilised. In the presence of rhombic splitting ($E \rightarrow 0$), the M_S states mix as E can mix with the states very strongly, which differs $\Delta M_S = \pm 2$.^[14] In the case of $S = 3/2$, E can mix $|+1/2\rangle$ with $|-3/2\rangle$ or $|-1/2\rangle$ with $|+3/2\rangle$ spin-orbit states. In the case of the $S=1$ system, E mixes the $|\pm 1\rangle$ states.

In the first-row TM series, although Co^{II} is the most popular metal ion to exhibit zero-field or field-induced SIM behaviour, other non-Kramers ions such as Mn^{III} , Fe^{II} and Ni^{II} -based complexes also found to be attractive. A major portion of our discussion is dedicated to Co^{II} -based SIMs for the following reasons i) they often form high-spin complexes in their native state (i.e., $S=3/2$ ground state), ii) they are relatively stable in varying coordination numbers (from 4 onwards), iii) being a Kramers ion, the ground spin-orbit M_S levels remain degenerate unless an external magnetic field is applied, thus offer the best choice to control/reduce the QTM, (iv) Kramers ions, such as Co^{II} can even exhibit slow relaxation of magnetisation with a positive D in the presence of a small applied dc field.^[15] Owing to these advantages, Co^{II} ions are the natural choice of SIMs among transition metals. As the orbital degeneracy of Co^{II} is lifted by the ligand field, it is important to understand how various coordination numbers and donor atoms play a role in controlling the ZFS parameter. Hence, we begin our discussion with Co^{II} complexes having larger coordination numbers and gradually move to low coordination numbers. Although there are some recent reviews on Co^{II} SIMs focusing on the synthesis and magnetic properties, here we aim mainly to discuss some of the recent developments of Co^{II} , Fe^{III} and Ni^{II} SIMs with large D or U_{eff} values where both theoretical and experimental studies have been carried out.^[5,16] We will also emphasise the theoretical methods used for several years to understand the magnetic anisotropy in transition-metal complexes and how the predictions made from computation has advanced the cut-

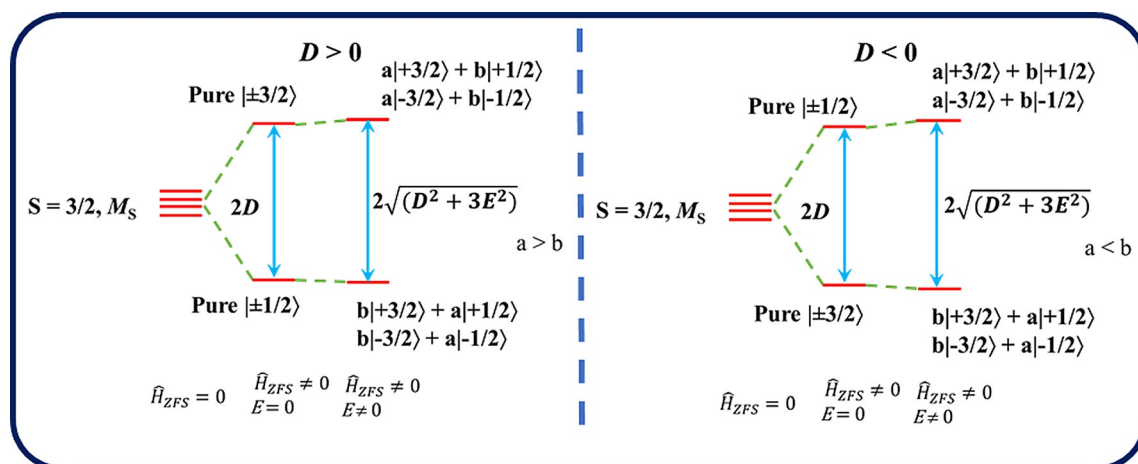


Figure 1. Depiction of the ZFS within the M_S manifold of $S=3/2$ spin system. On the left-hand side, the D is positive and on the right-hand side D is negative.

ting edge research in this area. The Co^{II} complexes are discussed by starting from higher coordination numbers to lower coordination numbers with special emphasis on endohedral cobalt-fullerene examples. In the case of Fe^{II} and Ni^{II} examples, we stress the geometry or coordination numbers where only negative D values have been achieved. How the geometry and electronic configuration influences the D and E/D parameters and where to search for complexes with high negative D values (with small E/D values) have been addressed in this review. Other early transition-metal complexes containing V^{III} , V^{II} , Cr^{III} , Cr^{II} , Mn^{III} and Mn^{II} have not been covered here as the number of SIM properties reported for these ions are rare as they exhibit smaller $|D|$ values. We also would like to mention here that the terminology of single-ion magnets used here and elsewhere in the literature is not strictly correct as there are always organic ligand backbones coordinated to the metal ion. The terminology “single-ion” thus here refers to single paramagnetic ions.

Co^{II} -based single-ion magnets

Eight- and seven coordinate Co^{II} SIMs

Among the higher coordination number complexes of Co^{II} , seven-coordinate complexes are very common and are widely studied whereas eight-coordinate complexes are rare. Almost all of the reported Co^{II} seven-coordinate complexes show field-induced SIM behaviour as they exhibit positive D values. The magnitude of D ranges from $+30 \text{ cm}^{-1}$ to $+60 \text{ cm}^{-1}$.^[17] They are not a popular choice for the construction of SIMs for this reason. However, owing to the Kramers nature of the ground state, it can show field-induced SIM behaviour and hence are fascinating examples to explore the magnetic properties through various ligand design strategies. Most of the seven-coordinate Co^{II} complexes are stabilised in pentagonal bipyramidal (PBP or D_{5h} symmetry) geometry or distorted PBP geometries. To mention $[\text{Co}(\text{H}_2\text{DAPBH})(\text{H}_2\text{O})(\text{NO}_3)]\text{NO}_3$ (**1**)^[18] (H_2DAPBH = 2,6-diacetylpyridine bis-benzoylhydrazone), $[\text{Co}(\text{H}_2\text{daps})(\text{MeOH})_2]$ (**2**)^[19] (H_2daps = 2,6-bis(1-salicyloylhydrazonoethyl) pyridine) and $[\text{Co}(\text{H}_2\text{L})(\text{NCS})_2](\text{SCN})_2$ (**3**)^[20] (H_2L = 2,2'-[2,6-pyridinediylbis(ethylidene-1-hydrazinyl-2-ylidene)]bis[*N,N,N*-trimethyl-2-oxoethanaminium]) complexes possess D values of $+35(31) \text{ cm}^{-1}$, $+38(43) \text{ cm}^{-1}$ and $+41(30) \text{ cm}^{-1}$, respectively, as revealed from NEVPT2 calculations and SQUID data (see Figure 2c–f). Ground state electronic configuration in these geometries can be represented by the $d_{xz}^2 d_{yz}^2 d_{x^2-y^2}^1 d_{xy}^1 d_{z^2}^1$ electronic configuration. Multi-configurational CASSCF/NEVPT2 calculations reveal that the ZFS arises dominantly from the first four spin-allowed excited ligand-field states and all four consist of different M_L valued electronic transition (see Figure 2a).^[18–21] It was found that the axial ligand donor strength and the equatorial ligand symmetry plays a very important role in determining the magnitude of the D value in these type of complexes. Particularly as the major contribution to D arises from different M_L level excitations, D is expected to be positive, and as the gap between the d_{xz}/d_{yz} to $d_{xy}/d_{x^2-y^2}$ decides the magnitude of D , it is expected to be only moderate. In this geometry, the $\Delta E(d_{xz}/d_{yz} - d_{xy}/d_{x^2-y^2})$ gap is directly correlated to the

ligand field splitting and is thus expected to be on the order of several thousand wavenumbers, reducing the prospect of obtaining larger D values. Out of these three complexes, only complex **2** shows $U_{\text{eff}} = 23 \text{ cm}^{-1}$ under an applied dc field. Very recently, a Co^{II} complex $[\text{Co}(\text{NO}_3)_2(\text{L})]$ (where L = ethyl-2,6-di(1-*H*-pyrazol-1-yl)isonicotinate) (**4**) has been reported by Sato and co-workers, which shows a temperature-dependent dynamic switching from seven- to six-coordinate geometry.^[22] The seven-coordinate structure is stabilised at low temperature (1–50 K) and six coordination at high temperature ($> 135 \text{ K}$). SQUID measurements and CASSCF/NEVPT2 calculations revealed a negative D value of -8.31 cm^{-1} for seven coordination and -31.45 cm^{-1} for six-coordinate geometry, and this suggests that negative D values can also be achievable for seven-coordinate geometry.

On the other hand, there are only a few Co^{II} eight-coordinated complexes reported in the literature where thorough magnetic characterisation and computation have been performed.^[23] Particularly, $[\text{Co}^{\text{II}}(12\text{-crown-4})_2](\text{I}_3)_2$ (**5**) shows a remarkable D value of -70 cm^{-1} from CASPT2 level of theory ($D_{\text{fit}} = -38 \text{ cm}^{-1}$) with an U_{eff} of 17 cm^{-1} (see Table 1).^[23a,b] Complex **5** possesses an S_8 symmetry axis around the Co^{II} centre and magneto-structural correlation revealed that the D value depends upon two structural parameters, namely the axial angle α and twist angle ϕ (see Figure 2g–h). The crystal field splitting pattern for an ideal square anti-prismatic (SAP) geometry (considering only the sigma bonding) is given in Figure 2b. As one can see here, the lowest energy transition is expected to occur between the d_{xy} to $d_{x^2-y^2}$ orbitals, and hence the D value is expected to be negative. In fact, the perfect square anti-prismatic geometry is expected to have Jahn–Teller distortions lifting the degeneracy between the d_{xy} to $d_{x^2-y^2}$ orbitals and any ligand design that could reduce the Jahn–Teller distortion is expected to yield very large negative D values as large as -106 cm^{-1} , as revealed from the theoretical calculations.^[23b] Later, Gao and co-workers also synthesised and characterised four eight-coordinated Co^{II} SIMs out of which the largest D value of -46.9 cm^{-1} (from CASPT2-RASSI-SO calculations) was revealed for the $[\text{Co}^{\text{II}}(\text{L})_2](\text{ClO}_4)_2$ (L = 2,9-dialkylcarboxylate-1,10-phenanthroline) complex (**6**), which was verified from dc susceptibility and magnetisation measurements.^[23c]

Six-coordinate Co^{II} SIMs

Six-coordinate Co^{II} complexes are common among Co^{II} ions and generally exhibit distorted octahedral (O_h) geometry, which possesses large $|D|$ values ($> 60 \text{ cm}^{-1}$) owing to the unquenched orbital contribution in the t_{2g} set and close-lying excited states (see Figure 3a). Except for some examples,^[24] most of the reported Co^{II} six-coordinate complexes with pseudo-octahedral geometry possess high positive D values with a significant E/D value.^[15,24a,25] Out of the few examples, the homoleptic pseudo-octahedral $[\text{Co}(\text{bpp-COOMe})_2](\text{ClO}_4)_2$ (where bpp-COOMe = methyl 2,6-di(pyrazol-1-yl(pyridine-4-carboxylate)) complex (**7**) reported by Rigamonti et al. possesses easy-axis anisotropy with a large negative D value of -86.2 cm^{-1} obtained from NEVPT2 calculations (see also Table 1).^[24b] This

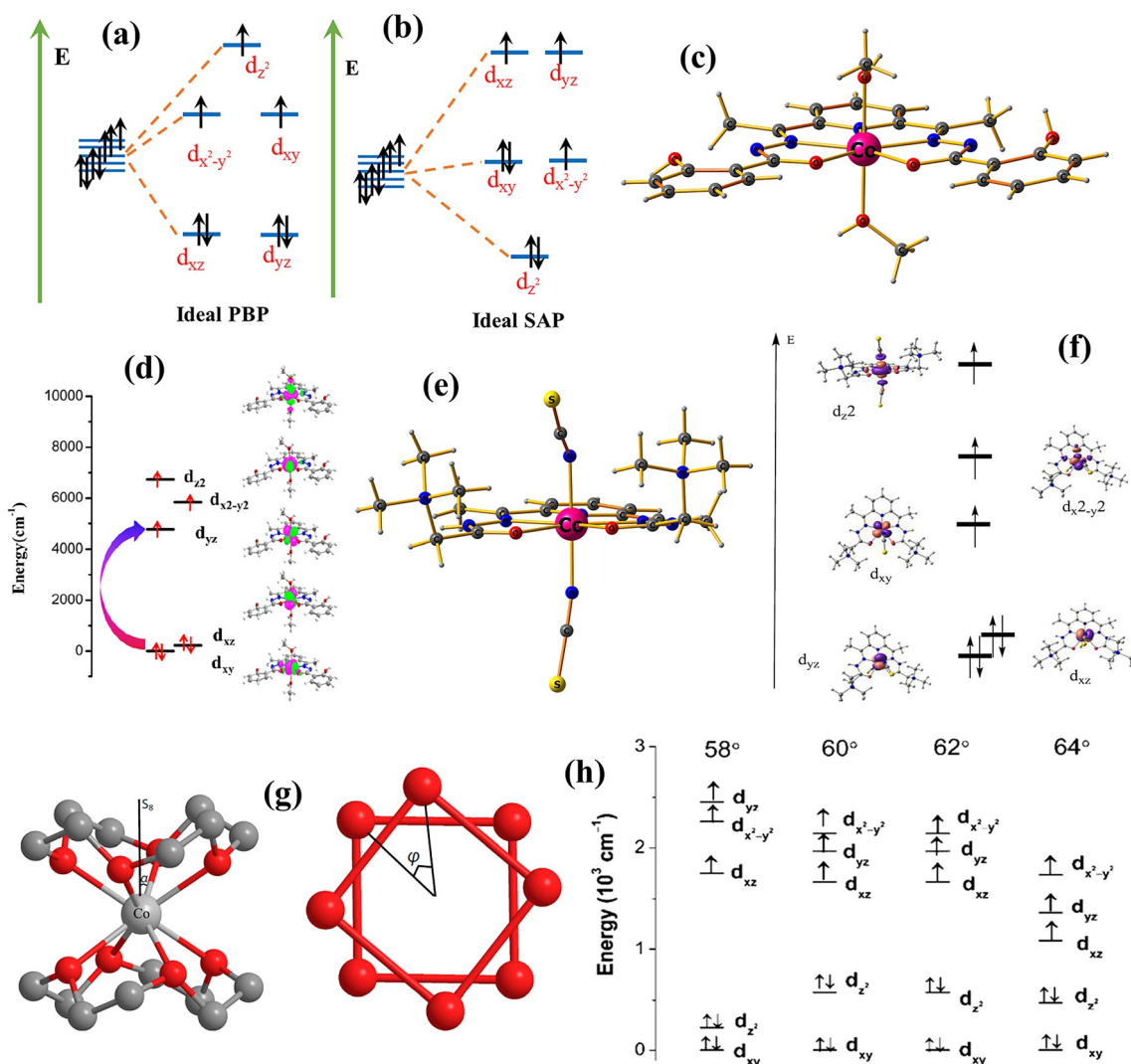


Figure 2. (a, b) Ideal PBP and SAP energy splitting of five d orbitals for d⁷ configurations, respectively. (c) X-ray structure of complex (2). (d) Ab initio ligand field (AILFT) energy splitting in complex (2). Reprinted with permission from ref. [19]. Copyright 2018 American Chemical Society. (e) X-ray structure of complex (3). (f) AILFT splitting diagram of 3d orbitals in complex (3). Reprinted with permission from ref. [20]. Copyright 2019 American Chemical Society. (g) X-ray structure of complex (5) side view and top view. The S_h axis along with two important structural parameters α and ϕ . (h) Variation of the 3d orbital energies with respect to the α parameter of complex (5). Reprinted with permission from ref. [23b]. Copyright 2015 American Chemical Society. Colour code: pink: Co; red: O; blue: N; grey: C; light grey: H; yellow: S; sky blue: Y; orange: P; light green: Si; brown-red: Fe; deep orange: Br; yellowish green: Cl; bluish green: Ni. The same colour code has been used throughout the review except in Figure 2g.

complex displayed field-induced (1000 Oe) SIM behaviour with $U_{\text{eff}} = 30.3 \text{ cm}^{-1}$. However, the dilution experiments revealed zero-field SIM behaviour owing to suppression of dipolar interactions. Also, there are some Co^{II} six-coordinated complexes reported in the literature where the geometry around the metal centres remains in the borderline region between octahedral and trigonal symmetry.^[24a] Mostly, isomeric meridional octahedral complexes show this unusual behaviour where D is negative despite a pseudo-O_h environment.

On the other hand, there are plenty of pseudo-O_h Co^{II} complexes that exhibit field-induced SIM behaviour attributed to positive D and large E/D values. For example, complexes *cis*-[Co^{II}(dmphen)₂(NCS)₂]^[15] (**8**) (dmphen = 2,9-dimethyl-1,10-phenanthroline) and [Co(μ-L)(μ-CH₃COO)Y(NO₃)₂]^[25h] (**9**) (L = ferrocene based compartmental ligand) were found to possess very

high easy-plane anisotropy with D values of +98 cm⁻¹ and +92 cm⁻¹ with small U_{eff} values of 17.0 cm⁻¹ and 7.6 cm⁻¹, respectively (see Figure 3b and Table 1). Very recently, Dunbar and co-workers reported three pseudo-octahedral complexes of general formula [Co(py)₄X₂]^[26] (where X = SCN, Cl and Br) out of which the Cl and the Br analogues (complexes **10** and **11**) exhibit very high D values of +127 cm⁻¹ and +139 cm⁻¹ as obtained from NEVPT2 calculations along with U_{eff} values of 19.3 cm⁻¹ and 20.4 cm⁻¹, respectively, in the presence of a dc field (see Figure 3c). Soon after, the same group reported another pseudo-octahedral complex [Co(MeCN)₆(BF₄)₂]^[27] (**12**) in which the D parameter (or B_2^0 parameter) was estimated to be +146.5 cm⁻¹ from NEVPT2 calculations (+148.9 cm⁻¹ from PHI fitting of the dc magnetic data) but with a smaller U_{eff} value of 7.6 cm⁻¹. The origin of this large positive D arises from the un-

Table 1. Comparison of the experimental and calculated ZFS parameters along with the U_{eff} values for all the discussed Co^{II} complexes. In most of the D_{cal} values, NEVPT2 or CASPT2 values are preferred over CASSCF values, if available.

Complex	D_{cal} [cm^{-1}]	$ E/D _{\text{cal}}$	D_{exp} [cm^{-1}]	$ E/D _{\text{exp}}$	U_{eff} [cm^{-1}] zero field	U_{eff} [cm^{-1}] in dc field	Ref.
1	35.4	0.06	31.0	0.00	–	–	[18]
2	38.0	0.09	43.1	0.09	–	23.3	[19]
3	41.5	0.05	30.0	0.00	–	–	[20]
4	–8.3	0.18	–8.01	0.31	–	–	[22]
5	–70.1	0.02	–38.0	0.00	–	17.0	[23a]
6	–46.9	0.11	–40.5	0.15	–	13.9	[23c]
7	–86.2	0.17	–57.5	0.27	–	30.3	[24b]
8	146.0	0.19	98.0	0.09	–	17.0	[15]
9	91.7	0.25	87.9	0.13	–	7.6	[25h]
10	127.0	0.15	68.2	0.14	–	19.3	[26]
11	139.2	0.02	61.5	0.11	–	20.4	[26]
12	146.5	0.18	148.9	0.15	–	7.6	[27]
13	63.3	0.15	57.0	0.31	–	17.0	[25a]
14	–107.0	–	–115.0	0.02	75.7	–	[29a]
15	–110.0	0.00	–109.0	0.00	71.0	101.0	[29b]
16	–97.3	0.00	–97.2	0.00	192.0	–	[31]
17	–113.6	0.02	–107.5	0.03	–	20.0	[31]
18	–150.6	0.00	–156.5	0.01	36.2	52.8	[27]
19	–114.5	0.15	–92.0	0.11	–	30.6	[29f]
20	–114.4	0.15	–93.0	0.12	–	44.7	[29f]
21	–62.1	0.17	–28.1	–	–	11.2	[34]
22	–121.7	0.14	–28.2	–	–	16.6	[34]
23	36.1	0.24	30.5	0.15	–	–	[32b]
24	40.1	0.24	46.4	0.22	–	26.2	[33d]
25	44.2	0.00	44.5	0.00	–	21.5	[32a]
26	–17.1	0.01	–21.4	–	–	–	[35]
27	–19.8	0.04	–20.2	–	–	21.0	[35]
28	–13.8	0.00	–11.0	–	–	20.0	[35]
29	–45.0	0.03	–70.0	0.09	21.0	–	[37]
30	–116.4	0.01	–161.0	0.00	33.9	–	[43]
31	–69.7	0.01	–80.7	0.01	62.0	–	[39c]
32	–117.8	0.02	–	–	–	–	[12c]
33	–112.0	0.01	–115.0	0.00	118	–	[44]
34	17.4	0.25	10.8	0.11	–	9.4	[41]
35	20.4	0.18	15.6	0.00	–	10.3	[40a]
36	–15.9	0.20	–11.3	0.00	–	20.2	[40a]
37	–	–	–57.0	0.23	–	16.1	[45]
38	–	–	–72.0	0.19	–	18.1	[45]
39	–	–	–82.0	0.00	–	19.1	[45]
40	40.6	0.01	40.2	0.00	–	29.2	[46]
41	–103.0	0.20	–85.4	0.11	–	26.0	[47]
42	–98.4	0.23	–80.6	0.16	–	–	[47]
43	210.1*	–	–	–	226	–	[48]
44	275.6*	–	–	–	297	–	[4b]
45	314.7*	–	–	–	288	–	[4b]
46	383.1*	–	–	–	413	–	[4b]
47	476.0*	–	–	–	450	–	[4a]
48	–118.5	0.00	–	–	–	–	[50]
49	–129.3	0.06	–	–	–	–	[50]
50	–115.0	0.04	–	–	–	–	[50]
51	–184.6	0.01	–	–	–	–	[50]
52	–148.1	0.03	–	–	–	–	[50]
53	–141.2	0.01	–	–	–	–	[50]
54	–150.1	0.04	–	–	–	–	[50]

* = corresponds to the energy gap between ground state KD and first excited KD.

quenched orbital angular momentum in the t_{2g} set of orbitals, which induces very strong spin-orbit coupling. Despite possessing such large $|2D|$ values, the U_{eff} values are small owing to the positive sign in D .

In the octahedral category, $[\text{Co}(\text{acac})_2(\text{H}_2\text{O})_2]$ complex (**13**) is an important example reported by Ruiz and co-workers with a

D value of $+63 \text{ cm}^{-1}$ (from CASPT2 calculations; see Figure 4a).^[25a] This is the first example to offer an insight into the mechanism of magnetisation relaxation in positive D Co^{II} complexes exhibiting SIM behaviour, prior to this report, it was believed that positive D complexes do not offer a barrier for the reorientation of magnetisation. In this work, detailed theoreti-

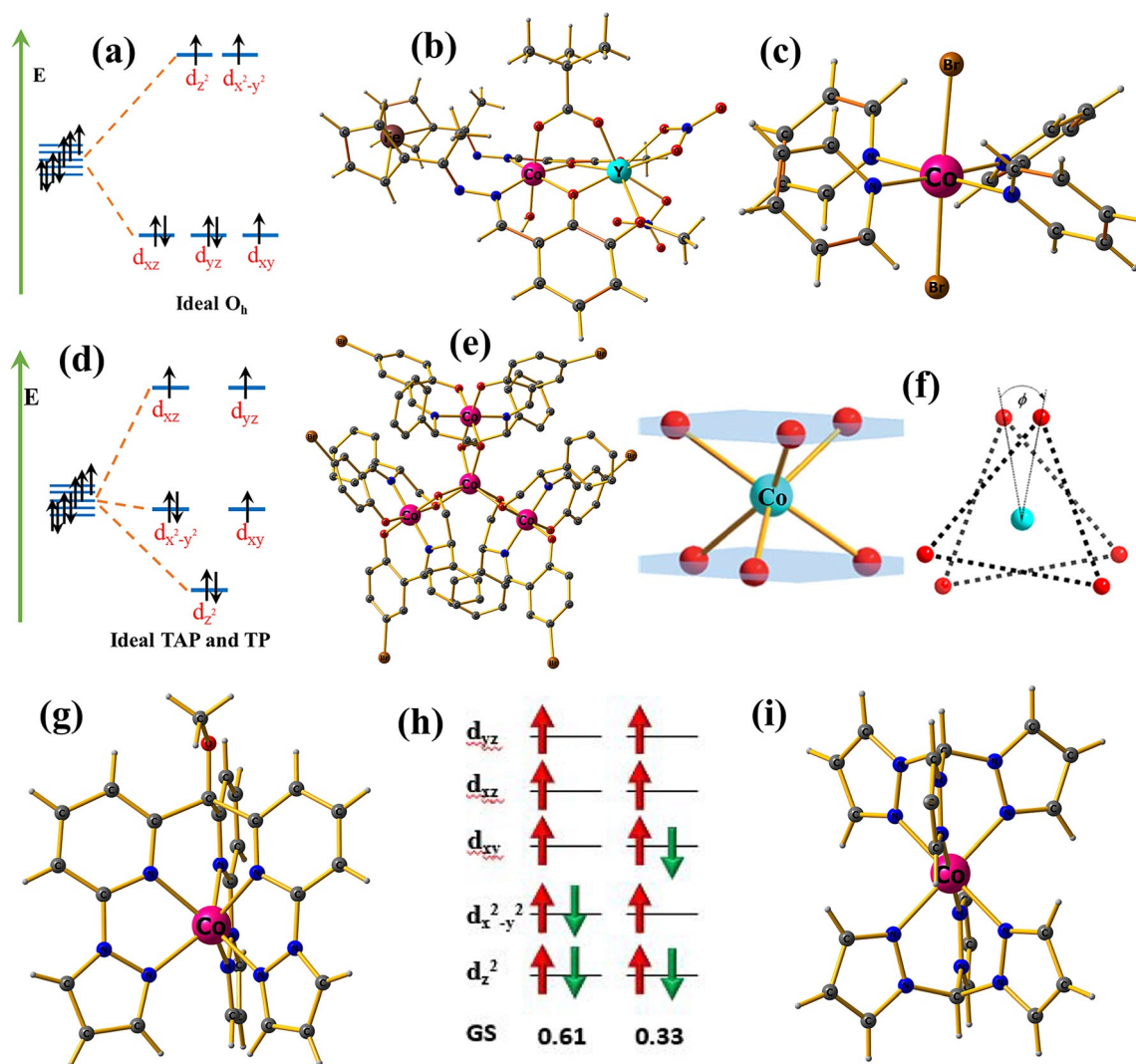


Figure 3. (a) Ideal d orbital splitting pattern for O_h geometry for d^7 electronic configuration. (b) X-ray structure of complex 9. (c) X-ray structure of complex 11. (d) Ideal d orbital splitting pattern in D_3 symmetry for d^7 electronic configuration. (e) X-ray structure of complex 14. (f) Arrangement of the two trigonal planes in complex 14. Reprinted with permission from ref. [29c]. Copyright 2015 American Chemical Society. (g, h) X-ray structure of complex 16 along with its multi-configurational character. (i) Crystal structure of complex 19 TAP arrangement.

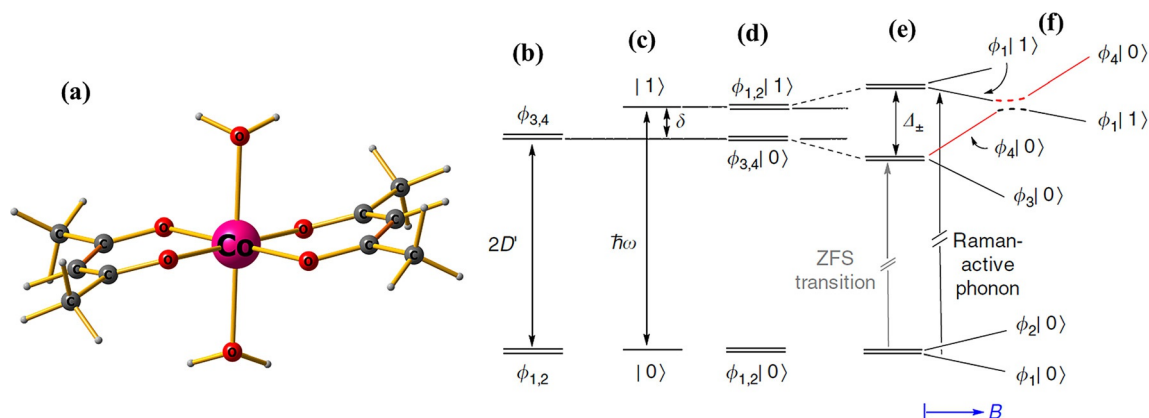


Figure 4. (a) X-ray structure of complex 13. (b) Separation between two Kramers pairs $\phi_{1,2}$ and $\phi_{3,4}$ in zero-field. (c) Uncoupled phonon states $|0\rangle$ and $|1\rangle$. (d) Spin-phonon product states with the Kramers pair without vibronic coupling. (e) Vibronic coupling leads to an energy shift and splitting by Δ_{\pm} . The ZFS transition here is of weak intensity in the Raman spectra as it is only magnetic dipole allowed. (f) Zeeman splitting of vibronic states during Raman active transitions showing avoided crossings. For further details, please see ref. [28].

cal calculations were performed to investigate the under barrier relaxation (or non-Orbach) mechanisms.^[25a] It was revealed that electronuclear spin entanglement is very important in intra-Kramers transitions, which opens up the QTM pathways and the relaxation processes in these complexes are dominated by a two-phonon Raman process. To compute the spin-phonon interactions, the following Pauli master equation has been solved [Eq. (5)]:

$$\frac{dP_n}{dt} = \sum_{\hat{n} \neq n} W_{n \leftarrow \hat{n}} P_{\hat{n}} - \sum_{\hat{n} \neq n} W_{\hat{n} \leftarrow n} P_n \quad (5)$$

where P_n is the time-dependent population of the electronuclear energy states $|\Psi_n\rangle$, and W refers to the transition rates between different states coupled by spin-phonon couplings. Both the electron spin-phonon and nuclear spin-phonon interactions have been considered to affect the relaxation mechanism. Later, Moseley et al. reported that the O-Co-O bond angle distortion plays a key role in the spin reversal mechanism through their spin-phonon studies on the same complex.^[28] They have also performed field-dependent Raman spectroscopic studies with a combination of ab initio calculations to show how the energy of the Kramers doublets mixes (avoided crossing) at the higher field, and this was the first direct observation of spin-phonon coupling in the Raman spectra at the molecular level (see Figure 4b–f). These under barrier relaxation or non-Orbach studies are essential as experimental barrier heights (U_{eff}) is smaller than the theoretically calculated values ($U_{\text{cal}} = 2\sqrt{(D^2 + 3E^2)}$) in most of the reported Co^{II} SIMs (see Table 1).

The trigonal prismatic (TP or D_{3h}) or trigonal anti-prismatic (TAP or D_{3d}) geometries are suitable for large and negative D values with a small E/D ratio and hence are expected to exhibit slow relaxation of magnetisation in zero applied dc field.^[29] It is the deviation towards the TP or TAP geometry from O_h geometry that decides the sign of the D value. This change in D takes place owing to alteration of the d orbital energies on moving from one geometry to the other. This is reflected in continuous symmetry measurements or SHAPE analysis performed on the complexes, which quantitatively measures the degree of deviation from ideal geometries.^[30] Also, deviation from ideal octahedral or TAP/TP geometries increases the multi-determinant character of the CASSCF wavefunction.^[25h] In TAP or TP geometries (D_3 point group or trigonal distortion), the d_{xy} and $d_{x^2-y^2}$ orbitals remain degenerate in d^7 electronic configuration, and consequently, a strong SOC leads to very large negative D values (see Figure 3d and 3h). Although there will be a weak Jahn–Teller distortion, which is expected to lift the degeneracy of these two orbitals, it is possible for a synthetic chemist to design a ligand that will minimise this Jahn–Teller effect. This fact is well established, particularly in five-coordinate Ni^{II} chemistry and has been reported in several theoretical as well as experimental reports.^[12a, 29e] Although the scenario here looks similar to the square anti-prismatic geometry in the eight-coordinate geometry, there are contrasting differences with D_{4d} being ideal, and deviation from D_{4d} towards cubic D_{4h} symmetry would lift the degeneracy of the $d_{xy}/d_{x^2-y^2}$ orbital,

leading to a drastic reduction in the D value. However, in the case of TAP/TP geometry, such distortion does not destroy the degeneracy, and hence it is still possible to obtain a negative D value.

First, a trigonal prismatic zero-field SIM was synthesised and studied by Gao and co-workers in 2013 where the main Co^{II} paramagnetic centre in (HNEt₃)[Co^{II}Co^{III}L₆]^[29a] (**14**) (L = H₂L = R-4-bromo-2-((2-hydroxy-1-phenylethylimino)methyl)phenol) possesses local D_3 symmetry (see Figure 3e) with a calculated D value of -107 cm^{-1} ($D_{\text{fit}} = -115 \text{ cm}^{-1}$). The U_{eff} for **14** was found to be a remarkable 76 cm^{-1} under a zero applied field, and this was the highest U_{eff} ever observed at that time. Later, the same group expanded their study on the family of [Co^{II}Co^{III}L₆] complexes, and even larger D values (from -140 cm^{-1} to -153 cm^{-1}) were obtained with very high U_{eff} values (from 89 cm^{-1} to 103 cm^{-1}) at the zero dc field.^[29c] It was found that as these type of complexes deviate from standard D_{3h} symmetry, the ZFS gets lower, and a perfect D_{3h} can result in a D as high as -160 cm^{-1} if the twist angle (φ) between the trigonal axis is maintained at zero degrees as predicted from calculations in model complexes (see Figure 3f).^[29c,e] The list of TP Co^{II} SIMs thus became very long, and several groups explored this geometry and designed various ligand architectures to achieve large negative D or U_{eff} values. Further, Winpenny and co-workers reported the rigid tris-pyrazolate cage complex [Co^{II}(Pzox)₃(BC₆H₅)Cl]^[29b] (**15**), which was characterised by magnetic measurements, NMR and ab initio calculations. A large negative D of -109 cm^{-1} (from NMR techniques) was obtained and confirmed from NEVPT2 results. This complex also showed a U_{eff} of 71 cm^{-1} at zero applied dc magnetic field (152 cm^{-1} for Orbach only) and 101 cm^{-1} at 1.5 kOe applied dc field. Following this path, very recently, Dunbar and co-workers investigated three TP Co^{II} SIMs, namely, [Co(tppm*)][BPh₄]₂ (**16**), [Co(hpy)][BPh₄]₂ (**17**) and [CoTp^{py}][PF₆] (**18**) (where tppm* = 6,6',6''-(methoxymethanetriyl)tris(2-(1-*H*-pyrazol-1-yl)pyridine); hpy = tris(2,2'-bipyrid-6-yl)methanol); Tp^{py} = tri(3-pyridylpyrazolyl)borate), which are the three best TP Co^{II} SIMs reported so far.^[27, 31] These three complexes exhibit D (or B_2^0) values of -97 (-97) cm^{-1} , -113.6 (-108) cm^{-1} and -151 (-157) cm^{-1} , respectively, for complexes **16**, **17** and **18** as obtained from NEVPT2 (PHI fitting of dc data) calculations (see Figure 3g). Very importantly, the U_{eff} values of 192 cm^{-1} (at zero dc field) in the case of complex **16** set a record for Co^{II} SIMs and is second only to the linear two-coordinate Co^{II} complexes (see also Table 1).^[31] The U_{eff} for complexes **17** and **18** are 20 cm^{-1} and 52.8 cm^{-1} (in dc field), respectively, and are much smaller compared with complex **16**. This can be attributed to the higher twist angle between the trigonal planes or rhombic anisotropy.

Among the trigonal anti-prismatic (TAP) examples of Co^{II}, very high negative D values were reported by Dunbar and co-workers for [Co^{II}(Tpm)₂][ClO₄]₂^[29f] (**19**) and [Co^{II}(Tpm)₂][BPh₄]₂^[29f] (**20**) (Tpm = tris(pyrazol-1-yl)methane) complexes possessing trigonal antiprismatic geometry (D_{3d} symmetry), which are worth a mention here. They exhibit a D value of -114 cm^{-1} as revealed by NEVPT2 calculations (see Figure 3i) for both the complexes. Owing to the presence of a higher order C_3 sym-

metry axis, these complexes also display low rhombic anisotropy (E/D) and thus are very good candidates to display zero-field SIM behaviour with attractive U_{eff} values.

Five-coordinate Co^{II} SIMs

Two types of coordination geometries are possible here: trigonal bipyramidal (TBP or D_{3h} point group) and square pyramidal (SqPy or C_{4v} point group) (see Figure 5a). Depending on the strength of ligand donation (σ - and π -), two types of splitting of the d orbitals can be envisioned in SqPy case. Owing to these variations, the D parameter can adopt two different signs, as depicted in Figure 5b. The majority of the Co^{II} five-coordinated SIMs show D values in the range $+35 \text{ cm}^{-1}$ to -20 cm^{-1} and most of them lie on the positive side of the scale.^[32] However, in some of the five-coordinate Co^{II} complexes, the D values were reported as being more than 40 cm^{-1} .^[32a,33] The first SIM of Co^{II} was reported by Murugesu and co-workers in 2011 in which two SqPy Co^{II} species $\{[\text{ArN} =$

$\text{CMe}_2(\text{NPh})\text{Co}(\text{NCS})_2$ (**21**) and $\{[\text{ArN} = \text{CPh}_2(\text{NPh})\text{Co}(\text{NCS})_2$ (**22**) were synthesised, characterised and both of them showed a D value of approximately 28 cm^{-1} (see Figure 5c).^[34] Both were characterised as field-induced SIMs, and ab initio CASSCF calculations by Ruiz and co-workers revealed D values of -62 cm^{-1} and -121 cm^{-1} for complexes **21** and **22**, respectively.^[13] Although the magnitude of the computed D is larger than the one obtained from the magnetisation data, it is imperative to stress here again that both the sign as well as magnitude of the D values are cumbersome to estimate from powder magnetisation data alone. Also, in the CASSCF calculations, the absence of dynamic correlation overestimates the D parameter and the addition of second-order (PT2) correction was found to improve the D significantly. In Figure 5c–e, three square pyramidal complexes are shown, of which complex (**21**) show a negative D of -28 cm^{-1} , whereas $[\text{Co}(\text{L})\text{Br}_2]$ ($\text{L} = 1$ -mesityl- N,N -bis(pyridine-2-ylmethyl)methanamine)^[32b] (**23**) and $[\text{Co}(\text{tris}[2\text{-(diphenylphosphino)ethyl]phosphine})\text{Cl}]\text{ClO}_4$ ^[33d] (**24**) exhibit positive D values of $+36 \text{ cm}^{-1}$ and $+40 \text{ cm}^{-1}$, respec-

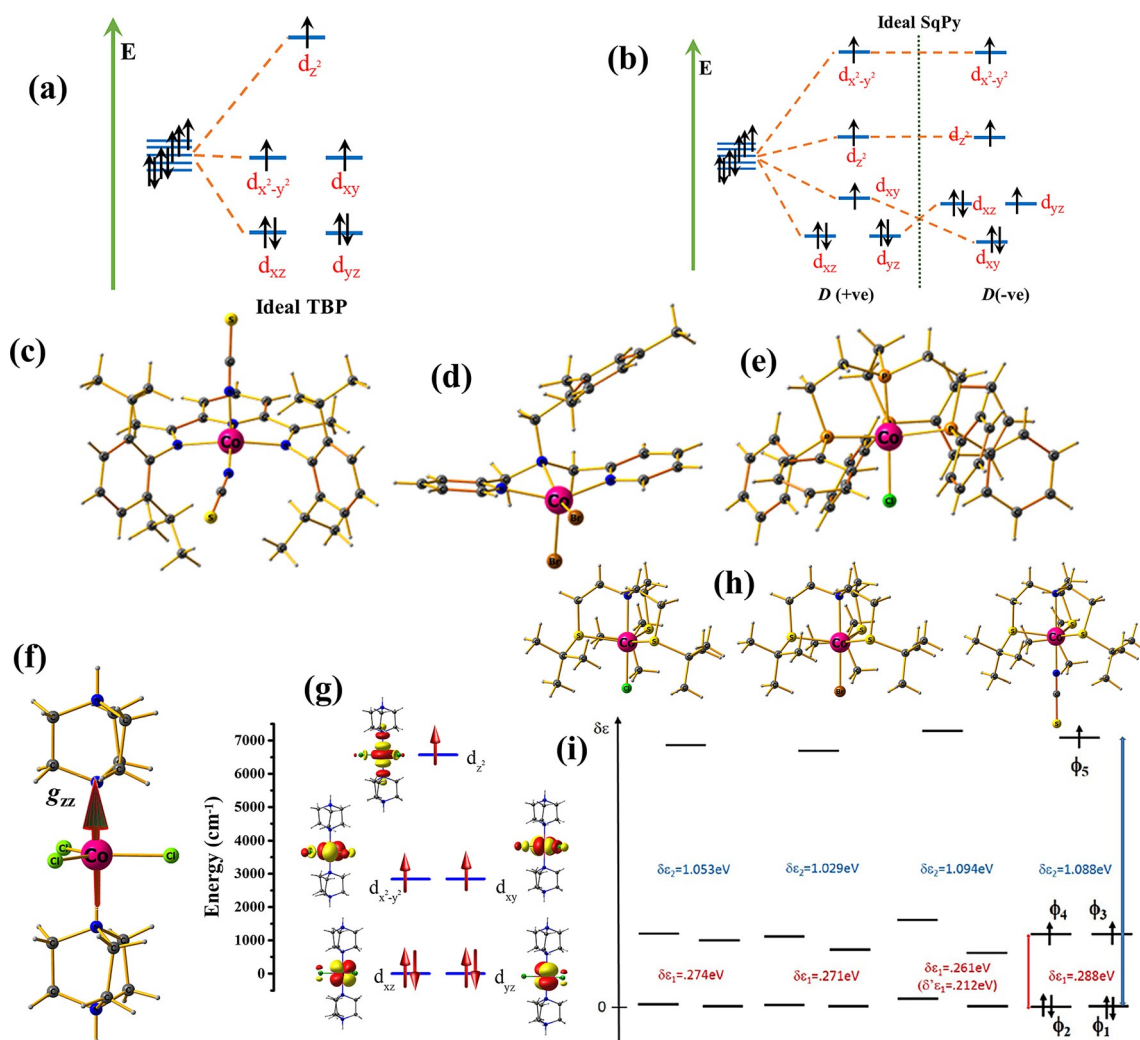


Figure 5. (a) Ideal d orbital splitting diagram in TBP geometry for d^7 electronic configurations. (b) Ideal square pyramidal d orbital splitting pattern with variation in D . (c) X-ray structures of complex (**21**), (d) of complex (**23**) and (e) of complex (**24**). (f) X-ray structure of complex (**25**) along with the NEVPT2 computed g_z axis. (g) NEVPT2-LFT computed d orbital splitting diagram of the same complex. (h) X-ray structure of three complexes (**26–28**). (i) CAS(7,10)SCF orbital diagram of the three complexes (**27** has two different unit cell structures). Reprinted with permission from ref. [35]. Copyright 2017 American Chemical Society.

tively, estimated from ab initio calculations and SQUID measurements.

On the TBP side, the $[\text{CoCl}_3(\text{DABCO})(\text{HDABCO})]^{32\text{a}}$ (**25**; DABCO = 1,4-diazabicyclo[2.2.2]octane) complex displayed a D value of $+44 \text{ cm}^{-1}$ as affirmed concurrently by HF-EPR spectroscopy and NEVPT2 calculations (see Figure 5 f–g). The estimate obtained from HF-EPR matches well with that from the NEVPT2 method, offering confidence in the methodology chosen. In this example, ab initio ligand field theory orbital (AILFT) analysis was performed, and the rhombic ZFS parameter (E/D) was found to be exactly zero. The additional calculations performed suggest that it is possible to obtain a negative D value as well for d^7 electronic configuration possessing TBP geometry. Guihéry and co-workers studied a series of TBP Co^{II} complexes $[\text{Co}(\text{NS}_3^{\text{tBu}})\text{X}]\text{ClO}_4$ ($\text{X}=\text{Cl}$ (**26**), Br (**27**) and NCS (**28**)) possessing C_{3v} symmetry with axial halide ligands.^[35] These complexes exhibit negative D parameters of -17 cm^{-1} , -22 cm^{-1} , and -14 cm^{-1} , respectively, and the sign of D can be rationalised from multi-determinantal ab initio calculations (see Figure 5 h).^[35–36] It was found that the transition from D_{3h} to C_{3v} symmetry helps to obtain a negative D parameter in these TBP Co^{II} complexes.^[36d] A softer donor ligand such as sulfur at the equatorial position was found to enhance the magnitude of D compared with other hard donor ligand atoms (see Figure 5 i). This work further emphasises the importance of multi-configurational CASSCF calculations to predict the sign as well as the magnitude of ZFS parameters in five-coordinated

Co^{II} complexes. It is to be mentioned here that all of the mentioned Co^{II} complexes display field-induced SIM behaviour.

Four-coordinate Co^{II} SIMs

Among the Co^{II} family, four-coordinate geometries are perhaps the most studied and well-explored to date. In an ideal tetrahedral (T_d) symmetry, the expected splitting pattern is shown in Figure 6 a, and here the D parameter is expected to be zero. However, geometric distortions from ideal T_d can offer significant D values as the excited states are closer in this geometry compared with octahedral and other higher coordination numbers. The range of D values can vary in this category from $+20 \text{ cm}^{-1}$ to -160 cm^{-1} . The geometry roughly varies from distorted tetrahedral (T_d or C_{2v}) to elongated tetrahedral (D_{2d}) structures. Again, one of the early works in TM-based SIMs started with pseudo-tetrahedral $[\text{Co}(\text{SPH})_4]$ (**29**) systems in 2011.^[37] Interestingly, accurate high-field EPR (HF-EPR) and dc magnetic measurements were performed on this complex way back in 1992,^[38] and the complex had to wait for another ten years to get the ac measurements carried out. In 2011, Long et al. carried out slow relaxation of magnetisation on complex **29** and showed that it exhibits one of the earliest examples of zero-field SIM.^[37] A thorough theoretical analysis performed by Neese et al. on this complex predicted a very large negative D value of -70 cm^{-1} .^[9a] Magneto-structural correlations performed on this type of $[\text{CoS}_4]$ system by us and others

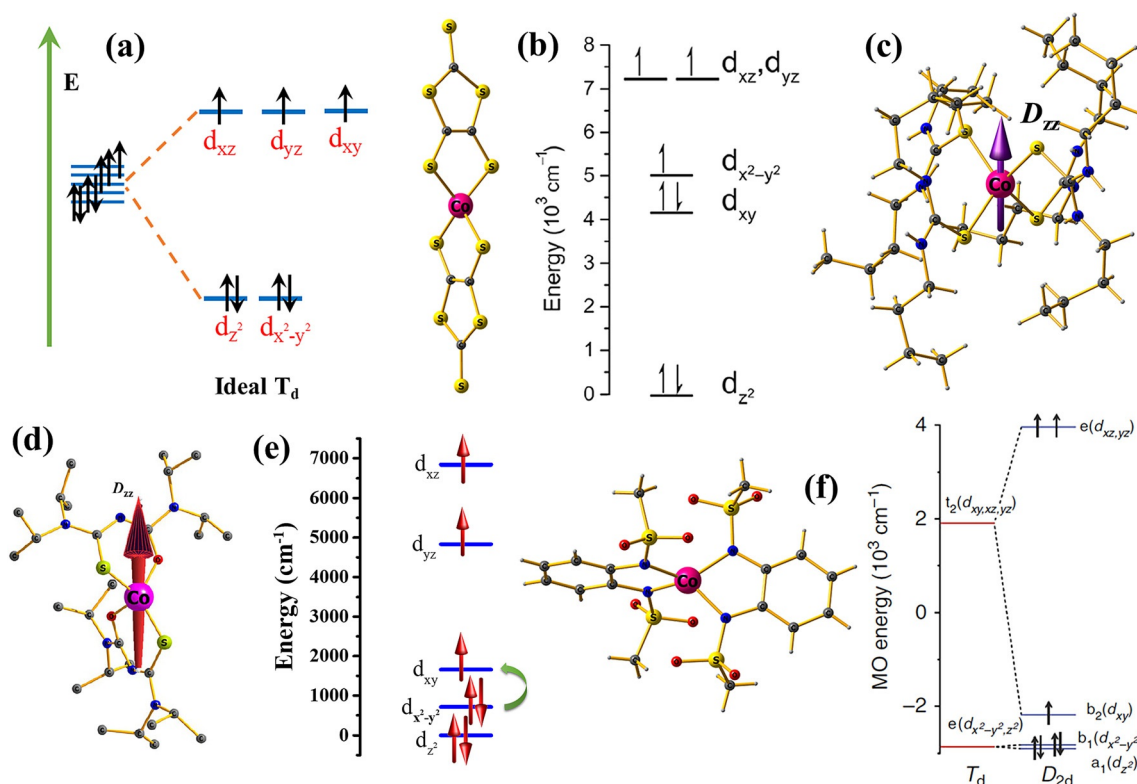


Figure 6. (a) Ideal d orbital splitting pattern in T_d geometry for d^7 electronic configurations. (b) X-ray structure of complex **30** along with the d orbital splitting diagram. Reprinted with permission from ref. [43a]. Copyright 2014 American Chemical Society. (c) X-ray structure of complex **31** along with the D_{zz} axis. (d) X-ray structure of complex **32** with the D_{zz} axis drawn on the structure. (e) AILFT computed d orbital splitting diagram of complex **32** (green arrow indicates the first excited electronic transition). (f) X-ray structure of complex **33** along with the NEVPT2 computed d orbital splitting pattern.

further revealed that the magnetic anisotropy of these complexes is controlled by the following factors: i) structural parameters such as bond angle and torsional angle around the first and second coordination sphere atoms,^[12c,39] ii) effect of donor atoms or ligand field strength,^[39b,40] iii) spin-orbit coupling of the donor atoms^[41] and also iv) counterions.^[39d,42] Soft donor groups such as S, Se/Br, I coordination bring down the ${}^4A_2 \rightarrow {}^4T_2$ (ligand field states in T_d symmetry) transition energy gap, and thus the D switches to negative from positive.

In 2014, the largest negative D in this category was reported by Freedman and co-workers with the $[\text{Co}(\text{C}_3\text{S}_3)_2]^{2-}$ (**30**) complex with a D value as high as -160 cm^{-1} (-114 cm^{-1} from SO-CASPT2 calculations), which still holds the record among four-coordinate Co^{II} systems to date (see Figure 6b).^[43] The large ZFS observed here is attributed to a perfect D_{2d} symmetry, which brings the $d_{x^2-y^2}-d_{xy}$ orbitals close to each other with no Jahn–Teller distortion and hence large D value. Most complexes having D_{2d} symmetry and lower E/D values exhibit zero-field SIM. In this regard, thiourea-containing ligands are important, and the $[\text{Co}(1,3\text{-dibutylthiourea})_4]$ (**31**) complex reported by Vaidya et al. showed a D value of -69.7 cm^{-1} ($D_{\text{fit}} = -80.7 \text{ cm}^{-1}$) with an U_{eff} of 62 cm^{-1} (in zero dc field) and hysteresis loop opening up to 4 K (see Figure 6c).^[39c] This U_{eff} value is the highest ever observed in the case of the $\{\text{CoS}_4\}$ core (see Table 1). Later, detailed ab initio calculations performed on $\{\text{CoO}_2\text{S}_2\}$, $\{\text{CoS}_4\}$ and $\{\text{CoSe}_4\}$ complexes revealed that if structural distortion occurs in the desired fashion, the D value can reach more than one hundred wavenumbers. Particularly, complex $[\text{Co}\{\text{N}(\text{SOCN}^{\text{Pr}_2})_2\}_2]$ (**32**) was found to yield a larger D value of -118 cm^{-1} ; this value was predicted by theory and has not yet been verified by experiments (see Figure 6d).^[12c] The d orbital splitting obtained from AILFT analysis reveals that the $d_{x^2-y^2}-d_{xy}$ gap is close to 940 cm^{-1} and the first excited quartet state lies only 417 cm^{-1} higher in energy (see Figure 6e). Other than S donor ligands, an N-coordinated Co^{II} complex ($\text{HN}(\text{Et}_3)_2[\text{Co}(\text{L})_2]$ (**33**) (where $\text{H}_2\text{L} = 1,2\text{-bis}(\text{methanesulfonamido})\text{-benzene}$), possessing again D_{2d} symmetry, was reported by van Slageren and co-workers, where a huge negative D value (-115 cm^{-1}) was confirmed from far-infrared spectroscopy, CASSCF-NEVPT2 calculations and other magnetic measurements (see Figure 6f).^[44] Complex **33** showed an U_{eff} of 118 cm^{-1} in a zero dc field, which is the best barrier height ob-

served for any four-coordinate Co^{II} SIM. Ultimately, it was found that maintaining the D_{2d} symmetry is key to achieving a large negative D value with four-coordinate Co^{II} complexes, and structural parameters always dominate over the soft or heavy atom substitutions.^[12c]

On the other hand, complexes having pseudo- T_d or C_{2v} symmetry exhibit smaller $|D|$ values compared with D_{2d} symmetric examples. The magnitude depends upon the first three excited-state energies, and the sign is determined by the orbital ordering upon ligand-field splitting. For example, complexes $[\text{Co}(\text{thiourea})_2\text{Cl}_2]$ ^[41] (**34**), $[\text{Co}^{\text{II}}(\text{L}^1)(\text{Cl})_2(\text{MeCN})]$ ^[40a] (**35**) ($\text{L}^1 = 2,3\text{-diphenyl-1,2,3,4-tetrazolium-5-olate}$) and $[\text{Co}^{\text{II}}(\text{L}^2)(\text{Cl})_2(\text{MeCN})]$ ^[40a] (**36**) ($\text{L}^2 = 2,3\text{-diphenyl-1,2,3,4-tetrazolium-5-thiolate}$) exhibit D values of $+17.4$ ($+10.8$) cm^{-1} , $+20.4$ ($+15.6$) cm^{-1} and -15.9 (-11.3) cm^{-1} , respectively, as obtained from ab initio CASSCF (SQUID) studies. In fact, complex **36** was first predicted and verified later, highlighting the constructive role of ab initio calculations in the design of Co^{II} SIMs.

Three-coordinate Co^{II} SIMs

Unlike four-coordinate complexes, three-coordinate Co^{II} complexes are rare in the literature. The geometry of the complexes reported are distorted trigonal planar (TP) geometries, and the expected qualitative d orbital splitting is shown in Figure 7a. Depending on the balance between the σ - and π -donor ability of the ligands, it can adopt two kinds of energy splitting, and subsequently, the sign of the D parameter can vary. In 2014, Andreas et al. reported three Co^{II} three-coordinate complexes $[\text{Li}(15\text{-crown-5})][\text{Co}\{\text{N}(\text{SiMe}_3)_2\}_3]$ (**37**), $[\text{Co}\{\text{N}(\text{SiMe}_3)_2\}_2(\text{THF})]$ (**38**) and $[\text{Co}\{\text{N}(\text{SiMe}_3)_2\}_2(\text{Pcy}_3)]$ (**39**), all of which displayed SIM behaviour under an applied dc field (see Figure 7b).^[45] Although fitting of the magnetisation data reveals negative D values of -57 cm^{-1} , -72 cm^{-1} and -82 cm^{-1} for **37**, **38** and **39**, respectively, ab initio CASSCF calculations performed on the model complexes could not unambiguously assign the sign of D as the E/D values are close to 0.33. Moreover, by looking at the field-induced ac signals, the sign of D could be positive and hence require further affirmative investigation such as HF-EPR or deeper ab initio analysis. The similar complex $[\text{Li}(\text{THF})_4][\text{Co}(\text{NPh}_2)_3]$ (**40**) with TP geometry exhibits a positive D value of $+40 \text{ cm}^{-1}$, which was confirmed from both

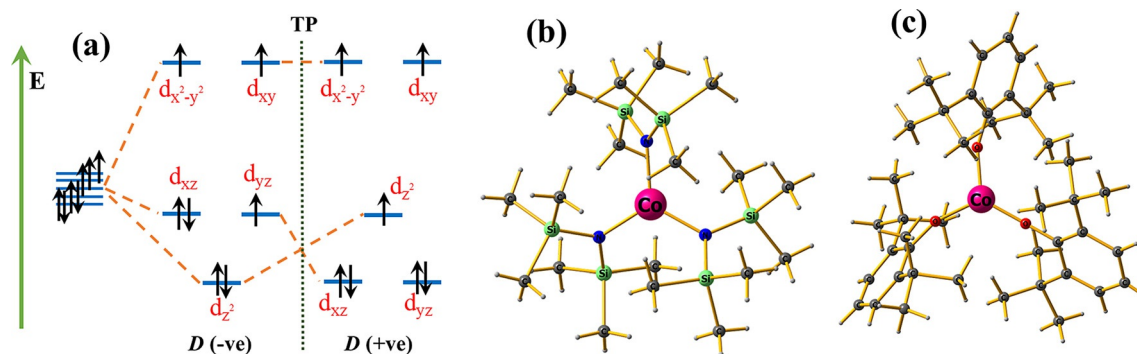


Figure 7. (a) Ideal trigonal planar d orbital splitting diagram for d^7 electronic configuration. (b) X-ray structure of complex **37**. (c) X-ray structure of complex **41**.

ab initio and dc magnetisation studies reported by Deng et al. in 2016.^[46] Interestingly, the same group reported two Co^{II} three-coordinated species with a {CoO₃} core: [Na(THF)₆][Co(Oar)₃] (**41**) and [(THF)₃NaCo(Oar)₃] (**42**), which exhibit negative *D* parameters of -103 cm^{-1} ($D_{\text{fit}} = -85\text{ cm}^{-1}$) and -98 cm^{-1} ($D_{\text{fit}} = -80\text{ cm}^{-1}$) obtained from NEVPT2 calculations (see Figure 7c).^[47] Perceiving these exciting results, further exploration is required in this category of complexes to understand the magnetic anisotropy deeper.

Two-coordinate Co^{II} SIMs

As reducing the coordination number reduces the crystal field splitting and enhances the anisotropy, there has been tremendous interest in the design and development of two-coordinate Co^{II} SIMs in recent years. As a Kramers ion is more effective for SIM than a non-Kramers, in 2013, the Long and Neese groups reported the large U_{eff} of 226 cm^{-1} ($U_{\text{cal}} = 210\text{ cm}^{-1}$) for a linear two-coordinate Fe^I complex [Fe(C(SiMe₃)₂)₂]¹⁻ (**43**) (*S* = 3/2 species) where slow relaxation of magnetisation has been observed in a zero field below 29 K.^[48] In 2016, Gao and co-workers reported three linear Co^{II} mononuclear complexes of the common formula [(NHC)CoNDmp] (where NHC = lPrNHC (**44**), cylPrNHC (**45**), sIPrNHC (**46**) and Dmp = 2,6-dimesitylphenyl) and among them complex **46** exhibits a record U_{eff} value of 413 cm^{-1} in zero applied dc field conditions.^[46] All three species contain strong Co=N double bonds along with bulky substituted NHC ligands, which helps to maintain a rigid linear geometry. Additionally, multi-reference DDCI3 calculations on top of the expanded active space of CAS(9,6) yielded 383 cm^{-1} energy separation between the ground Kramers doublets (KDs) and the first excited KDs. As the SOC is very large for the two-coordinate complexes, the term *D*, which is generally used to denote the splitting of *M_s* levels was not used. The anisotropy observed in such complexes is similar to that of lanthanides where spin-orbit splitting of various *M_J* levels account for the magnetic anisotropy. Recently, Long et al. reported a [Co(C-

(SiMe₂Onaph)₃]^[4a] complex (**47**), which showed a record U_{eff} of 450 cm^{-1} obtained from variable-field far-IR spectroscopy and ac magnetic susceptibility measurements and currently this complex holds the record for the largest U_{eff} reported for any transition metal SIMs (see Figure 8). Ab initio NEVPT2 calculations disclosed a non-Aufbau-type electronic configuration ($d_{x^2-y^2}, d_{xy}$)³(d_{xz}, d_{yz})³(d_{z^2})¹ with fully unquenched orbital angular momentum. Very strong first-order spin-orbit coupling separates the ground-state Kramers pair to the excited-state pair by 476 cm^{-1} as calculated from the NEVPT2 method.

Low-coordinate stable Co^{II} endohedral fullerenes

Despite the observation of large barrier heights of magnetisation reversal, the blocking temperature has not improved markedly for transition metal ion SIMs. Moreover, only low-coordinate Co^{II} SIMs exhibit extraordinary magnetic anisotropy and are worthwhile to compete with lanthanide SIMs; however, they also suffer from the same drawback that these are unstable under ambient conditions. In this regard, Co^{II} ions encapsulated in fullerenes as possible SIMs have been explored with the motivation from the report of very high blocking temperatures that arises from lanthanides encapsulated in fullerenes, which was originally predicted by ab initio calculations.^[49] Recently, similar Co analogues have been found to possess very large negative *D* parameters. A comprehensive theoretical study including DFT bonding analysis, molecular dynamics (MD) combined with modern CASSCF/NEVPT2 methods was performed on various sized Co endohedral metallofullerenes (Co-EMFs) starting from C₂₈ to C₈₂ cages to unravel the zero-field splitting on these next-generation potential SIMs.^[50] Initial calculations on Co@C₂₈ (**48**), Co@C₃₈ (**49**) and Co@C₄₈ (**50**) cages and their isomers revealed a negative *D* parameter of -129 cm^{-1} with a small rhombic *E/D* value for the Co@C₃₈ isomer (see Figure 9a and 9b). However, MD calculations carried out on the most stable isomers of Co@C₂₈, Co@C₃₈ and Co@C₄₈ disclose that there are more conformationally stable

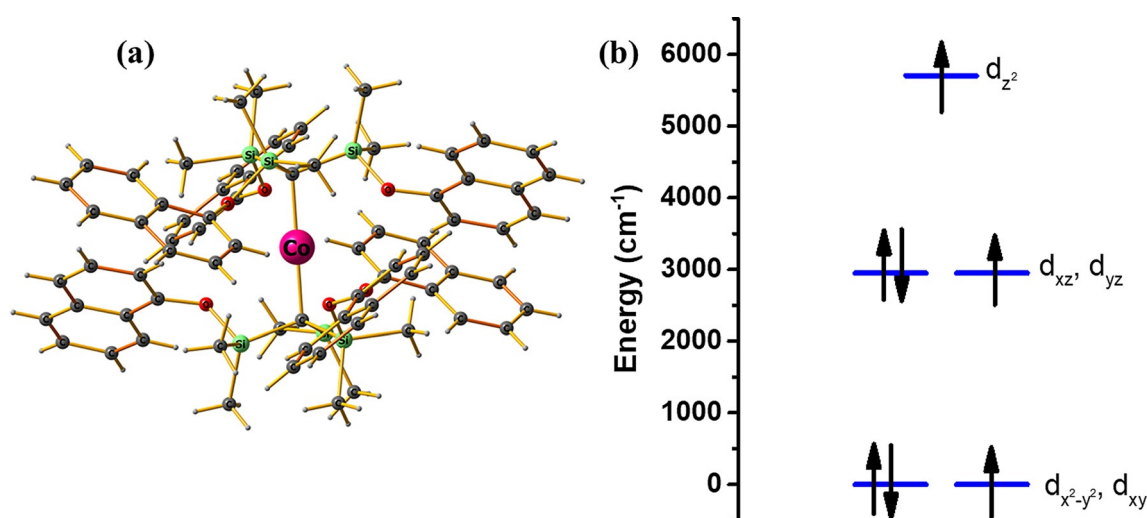


Figure 8. (a) X-ray structure of complex **47**. (b) Ab initio computed ligand field splitting pattern of the same, depicting non-Aufbau electron occupation.

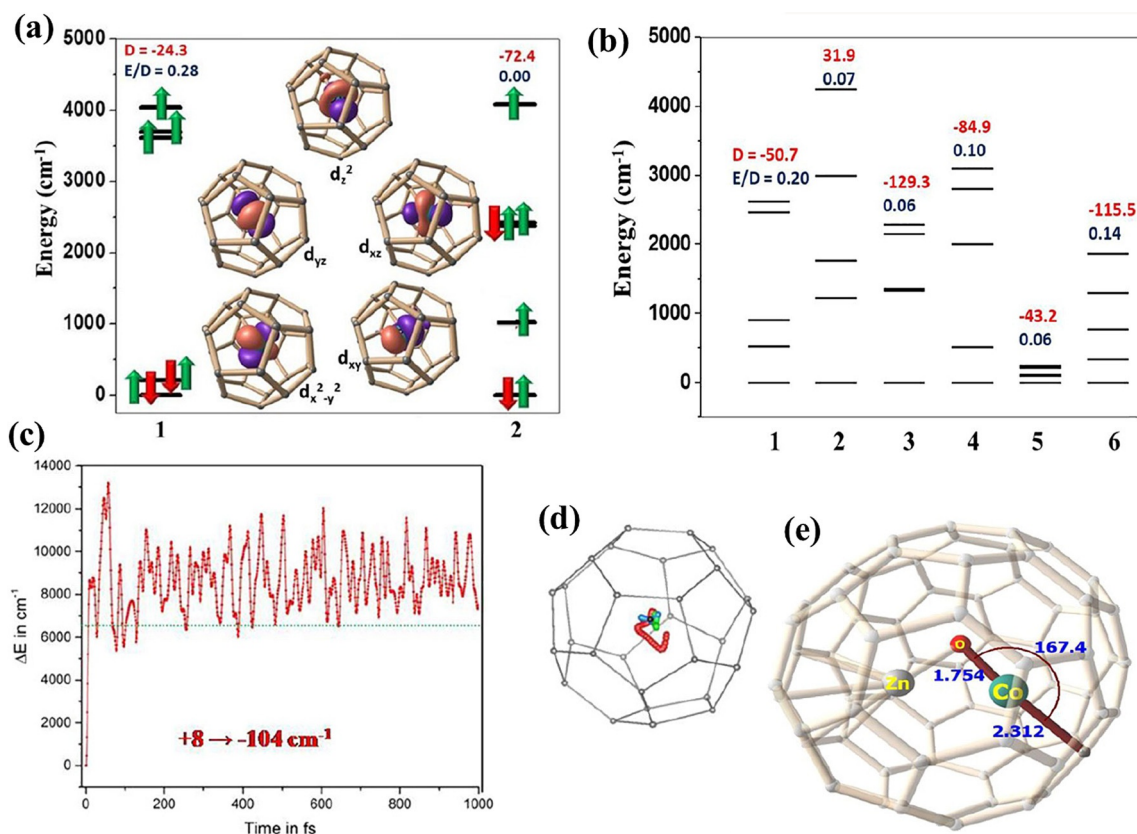


Figure 9. (a) NEVPT2 computed d orbital splitting diagram of the two most stable isomers of Co@C₂₈ cages and of (b) six stable isomers of Co@C₃₈ cages. (c) Time (in fs) evolution of total energy for the most stable isomer of Co@C₂₈ and (d) trajectory path of the Co ion inside the C₂₈ cage after the DFT-MD simulation (red, green and blue regions indicate the initial, intermediate and final stages of simulation). (e) DFT optimized structure of CoOZn@C₇₀. Reprinted with permission from ref. [50]. Copyright 2020 Wiley-VCH.

isomers possible for Co@C₂₈ cages compared with other cages and the D parameter can vary from +8 cm⁻¹ to -118 cm⁻¹ in Co@C₂₈ cages (see Figure 9c and 9d). Furthermore, to enhance the magnetic anisotropy in larger fullerene cages, diamagnetic ions and anions were inserted inside the cages to produce realistic models such as CoOZn@C₇₀ (**51**), CoOZn@C₈₀ (**52**), CoScZnN@C₇₆ (**53**) and CoScZnN@C₈₂ (**54**) (see Figure 9e). A significant increase in the calculated D value was encountered with these models as CoOZn@C₇₀ and CoZnScN@C₈₂ cages exhibited huge D values of -185 cm⁻¹ and -150 cm⁻¹, respectively, with negligible E/D values and are thus proposed as ideal candidates to obtain air-stable SIMs possibly with high blocking temperatures (see Figure 10). A comparison between the coordination number, geometry and the calculated D values of the discussed Co^{II} complexes are shown in Figure 11.

Fe^{II}/Fe^{III}-based single-ion magnets

Fe^{III} single-ion magnets

Among Fe^{II} and Fe^{III} high-spin complexes, preferably Fe^{II} shows slow relaxation of magnetisation as it has lower energy spin-allowed excited states compared with Fe^{III}, where spin-flipped excited states are accessible only at very high temperatures. Therefore, Fe^{II} (d⁶ system) is a clear choice over Fe^{III} (d⁵ system) for SIM applications, and expectedly there are numerous Fe^{II}

complexes reported to exhibit SIM properties compared with very few numbers of Fe^{III} examples. However, if the Fe^{III} ion can be stabilised in an intermediate $S=3/2$ state with the application of a strong ligand field, then it can behave similarly to high-spin Co^{II} and hence can exhibit strong anisotropy.^[51] Recently, Feng et al. stabilised two intermediate trigonal bipyramidal Fe^{III} complexes, [(PMe₃)₂FeCl₃] (**55**) and [(PMe₂Ph)FeCl₃] (**56**) with strong phosphorus coordinating axial ligands and studied their magnetic properties (see Figure 12a–c).^[51b] The D parameter for these two complexes was estimated to be -50 cm⁻¹ (**55**) and -17 cm⁻¹ (**56**), respectively, and for complex **54**, this was the highest D as well as U_{eff} observed for any Fe^{III} complex reported (see Table 2). Later, Roy Chowdhury et al. calculated the ZFS parameters on these two complexes with CASSCF/CASPT2 level of theory, and the computed D values were found to be -40.3 cm⁻¹ (for **55**) and -20.9 cm⁻¹ (for **56**), which almost exactly reproduces the experimental data.^[52] Not only that, they have also expanded the active space to CAS(9,7) during the multi-configurational calculations to include two phosphorus p_z orbitals to account for further electron correlation.

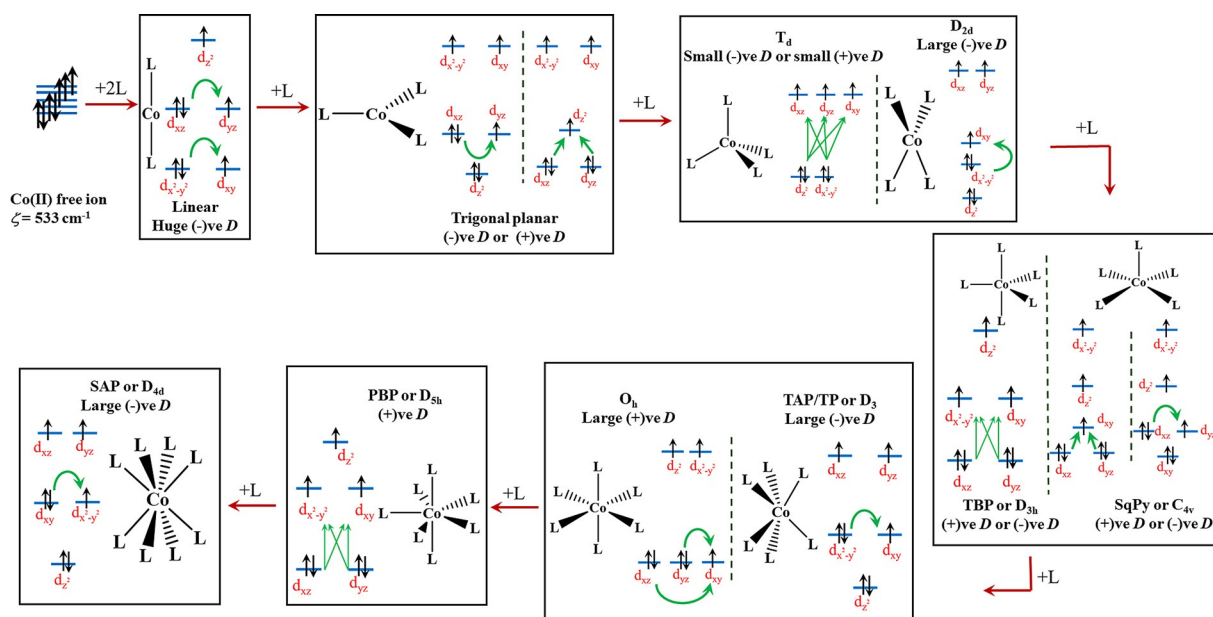


Figure 10. Schematic representation of the successive addition of ligands and their respective change in the qualitative d orbital splitting pattern along with the prediction of D values in the Co^{II} system. The green arrows indicate the lower energy electronic transitions responsible for ZFS.

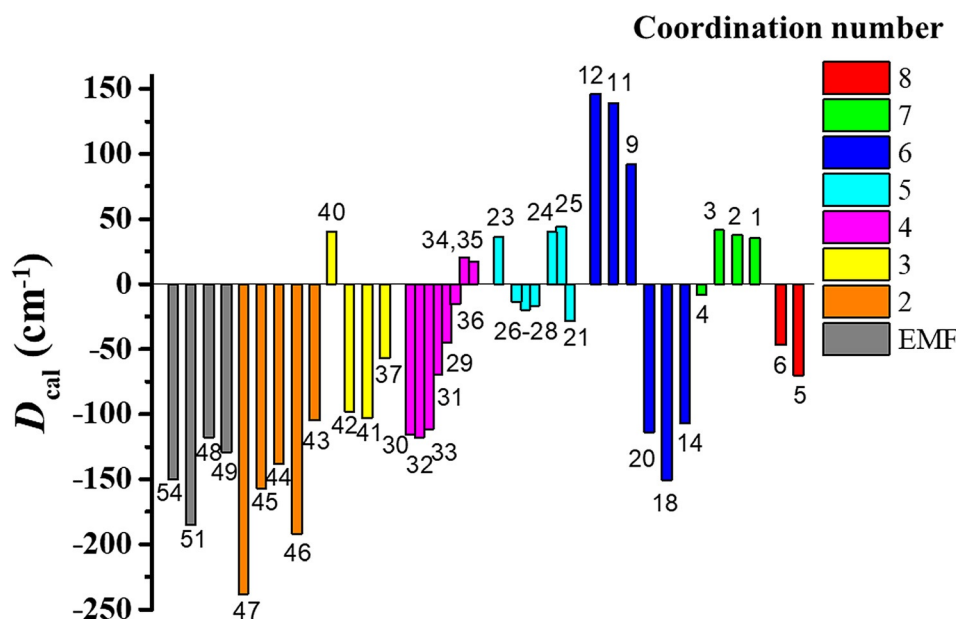


Figure 11. Bar diagram representation of the variation of D_{cal} values of selected Co^{II} complexes with respect to different coordination numbers (complex number written below the bars). In some of the cases, experimental D values are given, as NEVPT2 or CASPT2 has not been performed and CASSCF values are overestimated. In two-coordinate cases the D values are approximated by dividing the first excited KD energy by a factor of two.

Fe^{II} -based single-ion magnets (octa-, hepta- and hexa-coordinate complexes)

Among the Fe^{II} complexes, the observation of SIM behaviour is less compared with the Kramers ions as now the transverse or rhombic anisotropy (E/D) directly controls the tunnel splitting (in ± 2 and ± 1 M_S levels) and hence even small E/D (or E) leads to significant quantum tunnelling of magnetisation.^[53] Therefore, despite showing large magnetic anisotropy, the U_{eff} values are small, and therefore all reported complexes exhibit

are field-induced magnets. Also, positive ZFS (or positive D) in $S=2$ and $S=1$ systems have no magnetic importance as they form an anisotropic well via the non-magnetic $M_S=0$ ground state instead of an anisotropy barrier. The number of Fe^{II} SIMs is thus very small, and among them, high coordination number Fe^{II} complexes showing slow relaxation of magnetisation are even smaller. One of the earliest Fe^{II} heptacoordinated SIMs was reported to be in three pentagonal bipyramidal geometry by Bar et al. in 2015 with dc magnetic studies, ac measurements and Mossbauer studies.^[54] Later, detailed theoretical

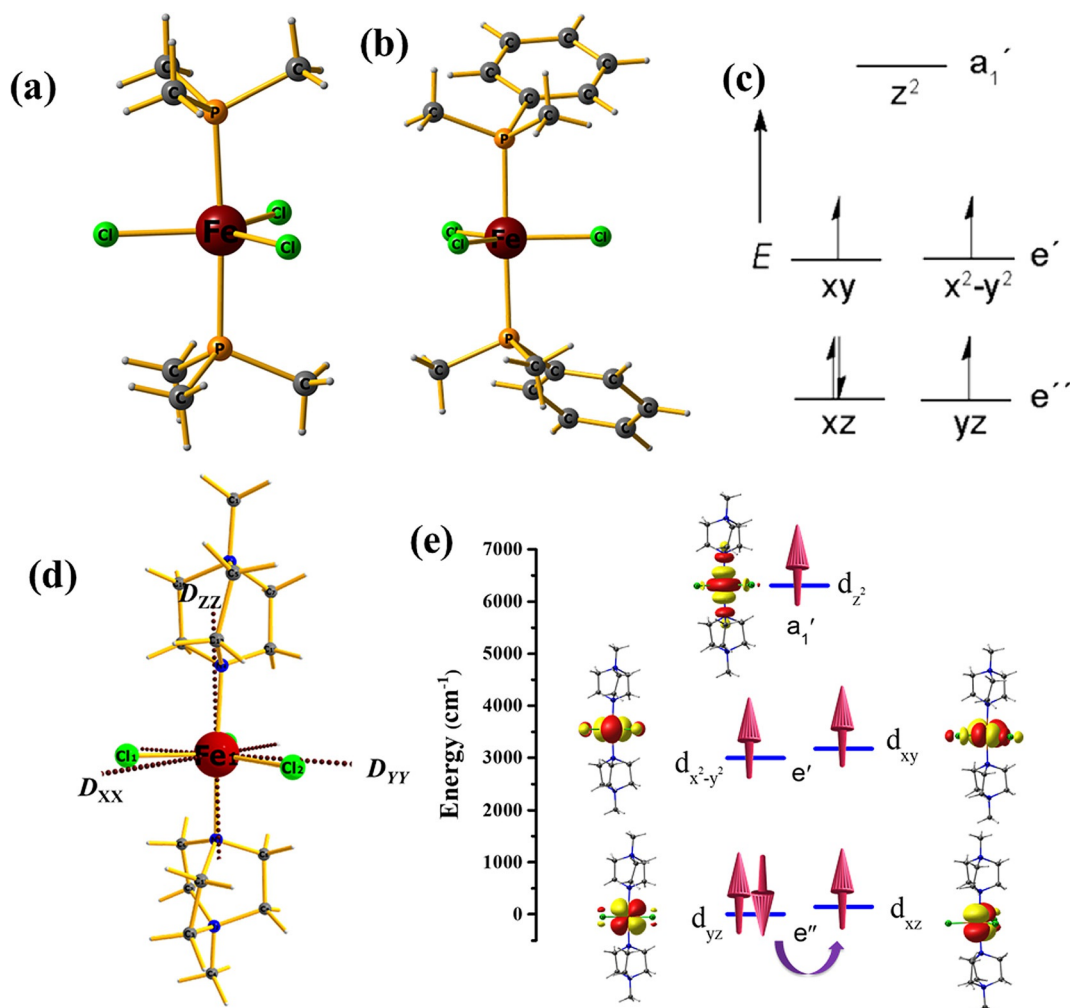


Figure 12. (a) X-ray structure of complex **55** and of (b) complex **56**. (c) Qualitative d orbital splitting of intermediate d^5 electronic configuration. Reproduced with permission from ref. [51b]. Copyright 2017 American Chemical Society. (d) X-ray structure of complex **66** with the major anisotropy axes drawn. (e) AllFT d orbital splitting diagram of complex **66** showing the first excited state electronic excitation.

Table 2. Comparison of the experimental and calculated ZFS parameters along with the U_{eff} values for all the discussed $\text{Fe}^{\text{II}}/\text{Fe}^{\text{III}}$ and Ni^{II} complexes. In most of the D_{cal} values, NEVPT2 or CASPT2 values are preferred over CASSCF values, if available. Also, HF-EPR data is preferred over dc magnetic data.

Complex	D_{cal} [cm^{-1}]	$ E/D _{\text{cal}}$	D_{exp} [cm^{-1}]	$ E/D _{\text{exp}}$	U_{eff} [cm^{-1}] in dc field	U_{cal} [cm^{-1}]	Ref.
55	−40.3	0.00	−50.0	0.00	81.0	—	[51b,52]
56	−20.9	0.01	−17.0	0.00	46.0	—	[51b,52]
57	−21.6	0.04	−13.3	0.01	37.0	—	[55]
58	−11.7	0.01	−11.7	0.01	19.0	—	[56]
60	—	—	—	—	146.0	196	[57,58]
61	—	—	—	—	104.0	161	[57,58]
62	−36.0	0.00	−47.5	0.00	65.0	—	[58,59]
63	—	—	−7.6	—	29.0	—	[62]
64	—	—	4.1	—	—	—	[62]
65	−13.7	0.01	−12.3	0.00	27.0	—	[64]
66	−27.5	0.02	−27.5	0.02	36.7	—	[65]
67	−16.8	0.07	−12.6	0.12	—	—	[18]
68	−43.5	0.03	−28.2	0.06	—	—	[67]
69	−14.7	0.09	−15.4	—	—	—	[68]
70	−205.0	0.01	−180.0	0.00	—	—	[8]
71	−244.0	0.01	−200.0	0.01	—	—	[69]
72	−400.0	0.00	−535.0	0.00	19.3	—	[70,12a]
73	−428.9	0.00	−276.0	0.01	—	—	[71]

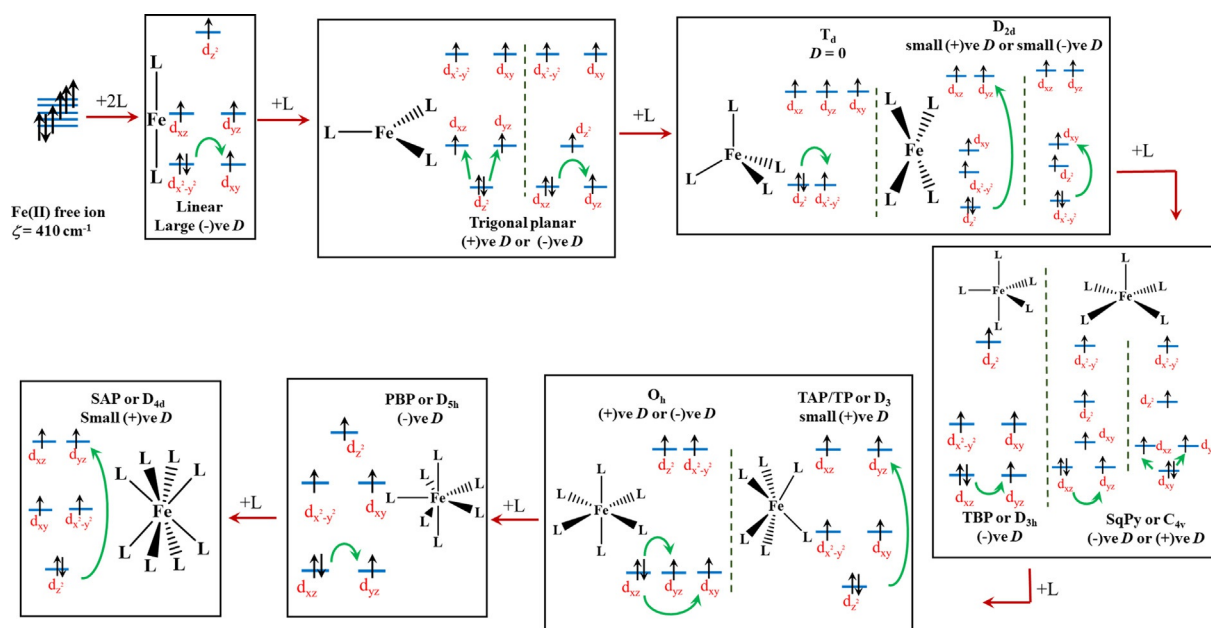


Figure 13. Schematic representation of successive addition of ligands and their respective change in the qualitative d orbital splitting pattern along with the prediction of D values in the FeII system. The green arrows indicate the lower energy electronic transitions responsible for ZFS.

calculations performed on these series of PBP-type Fe^{II} complexes reveal a small negative D parameter in all PBP complexes. For example, [Fe(H₂DAPBH)Cl₂] complex (**57**) showed a D value of -13.3 cm^{-1} from dc measurements (-21.6 cm^{-1} from CAS(6,5)NEVPT2 calculations) with an U_{eff} of 37 cm^{-1} .^[55] The origin of negative D can be clearly understood from the orbital splitting pattern in PBP (or D_{5h}) geometry for a d^6 system as the same M_L level valued $d_{xz} \rightarrow d_{yz}$ electronic excitation remains close to the ground state and contributes to the negative D significantly (see Figure 13).

Gao and co-workers have reported some Fe^{II} eight-coordinate SIMs in recent years, particularly, the [Fe^{II}(L)₂](ClO₄)₂ (where L = 1,10-phenanthroline-2,9-dicarboxylic acid) complex (**58**) is important as it shows a negative D of -11.7 cm^{-1} (from CASPT2-RASSI-SO) with U_{eff} value of 19 cm^{-1} .^[23c,56] To the best of our knowledge, there are no six-coordinate Fe^{II} SIMs reported to date.

Fe^{II}-based single-ion magnets (penta-, tetra-, tri- and two-coordinate complexes)

Among the low-coordinate Fe^{II} complexes, five-, three- and two-coordinate mononuclear complexes are common. The first two-coordinate Fe^{II} complex showing single-ion magnetism was studied by Reiff et al. in Fe[C(SiMe₃)₃]₂ (**59**) and Fe[N(tBu)₂]₂ (**60**) complexes and by Power et al. in [Fe(N(H)Ar*)₂]₂ (Ar* = C₆H₃-2,6-(C₆H₂-2,4,6-*i*Pr₃)₂) (**61**) complexes with two different aryl substituents.^[57] All three two-coordinate complexes have been experimentally characterised by Mossbauer, EPR and dc magnetometric measurements. But estimation of the ZFS parameters has not been reported as ac susceptibility measurements, and ab initio calculations were absent at that time. Later on, slow relaxation of magnetisation (in the presence of

an applied dc field) from ac measurements was observed by Long and co-workers in a family of trigonal pyramidal complexes reported in 2010.^[58] To stabilise such low-coordinate structures, and also to minimise the Jahn–Teller effects, bulky groups needed to be introduced into the ligand framework. HF-EPR and magnetic studies revealed a very high negative D value of -48 cm^{-1} in the trigonal pyramidal [(tpa^{tBu})Fe]⁻ (**62**) complex.^[58b] Theoretical investigation of this type of complex was not a trivial task. Neese et al. showed later how to treat these species having near orbital degeneracies with detailed ab initio methods combined with ligand field theory (AILFT) and angular overlap model (AOM).^[59] Specially, pseudo-linear Fe^{II} complexes overcome the Jahn–Teller distortion and show large U_{eff} or U_{cal} values and cannot be described by second-order ZFS or the traditional D parameter (see Table 2). The CASSCF/NEVPT2 calculations very nicely explained the origin of magnetic anisotropy, and the computed barrier heights (U_{cal}) were compared with the U_{eff} values (see Table 2). In addition, chemical bonding, vibronic coupling calculations were also performed to understand the relaxation mechanism and dynamics of magnetisation behaviour. Recent reports on the investigation of under-barrier relaxation on a similar $S=2$ Fe^{II} SIM [(tpa^{Ph})Fe]⁻ depicts the role of anharmonic phonons in the magnetisation relaxation mechanism.^[60] Lunghi et al. have illustrated the importance of phonon modes by calculating all the possible lattice/phonon vibrational frequencies of the unit cell of the complex with an ab initio approach.^[60] Their study reveals these anharmonic phonon vibrations are crucial to explain the relaxation mechanism and are strongly coupled to the spin dynamics at the high temperatures.

One of the earliest high-spin Fe^{II} three-coordinate complexes possessing large magnetic anisotropy was reported by Holland and co-workers in 2002.^[61] One of the complexes with the for-

mula $[(\beta\text{-diketiminate})\text{Fe}^{\text{II}}\text{CH}_3]$ is found to show a huge D value of -100 cm^{-1} from Mossbauer experiments. However, ac/dc measurements, ab initio calculations have not been performed on these complexes to unfold the nature of ZFS. These type of three-coordinate complexes have been studied by the same group for a long time for different applications such as reactivity for small molecule activation and catalysis. In 2011, Murugesu and co-workers reported two Fe^{II} SIMs, $[\text{Fe}(\text{N}(\text{TMS})_2)_2(\text{PCy}_3)]$ (**63**) and $[\text{Fe}(\text{N}(\text{TMS})_2)_2(\text{depe})]$ (**64**) (where $\text{depe} = 1,2\text{-bis}(\text{diethylphosphino})\text{ethane}$), of which complex **63** showed out-of-phase ac signals at an applied dc field with an U_{eff} of 29 cm^{-1} .^[62] The D values from dc measurements were estimated to be -7.6 cm^{-1} and 4.1 cm^{-1} for complexes **63** and **64**, respectively. Although no ab initio analysis has been carried out in this work, the positive D in complex **64** may be attributed to the different orbital splitting, and also it is four-coordinate rather than three-coordinate as in complex **63**. Four-coordinate Fe^{II} SIMs have been thoroughly investigated by us and others to probe the origin of magnetic anisotropy.^[53,63] It was found that both positive and negative D values can be obtained in four-coordination Fe^{II} systems depending on the dihedral or interplanar angle. From the negative D valued Fe^{II} SIMs, Werncke et al. have studied three four-coordinate complexes, of which $[\text{Fe}(\text{N}2\text{mes})_2]$ complex (**65**) (where $\text{N}2\text{mes} = 2\text{-[mesitylamino)methyl]pyridine}$) exhibited a D value of -13.7 cm^{-1} (from NEVPT2 calculations) with $U_{\text{eff}} = 27\text{ cm}^{-1}$ (see Table 2).^[64]

Very recently, Hay et al. reported the first trigonal bipyramidal Fe^{II} complex, $[\text{FeCl}_3(\text{MeDABCO})_2]\text{ClO}_4$ ^[65] (**66**), which shows a D value of -27.5 cm^{-1} obtained from NEVPT2 calculations and also from dc measurements. As expected, the U_{eff} is very small 36.7 cm^{-1} and 9.6 cm^{-1} in the presence of 600 Oe and 2500 Oe applied fields, respectively. The origin of this large negative D value is found to arise from the mixing of the first excited state, which lies 137 cm^{-1} above the ground state and corresponds to the $d_{yz} \rightarrow d_{xz}$ electronic transition (see Figure 12 d–e).

Ni^{II} -based single-ion magnets

The ion that can show perhaps the largest possible ZFS is the Ni^{II} system because it has the highest SOC constant ($\zeta = 649\text{ cm}^{-1}$). It has a non-Kramers ground state and very strong mixing between the $M_S = \pm 1$ level via E (or E/D) makes it somewhat unfavourable for showing SIM behaviour even if the D is negative. Therefore, this category of examples shows no or very small U_{eff} values. Still, there are viable ways to minimise this quantum tunnelling between the ± 1 level (in the case of negative D values). With a handful of examples of Ni^{II} SIMs, we are going to discuss here the most important examples covering seven-, six-, five- and four-coordination numbers showing negative D parameters. The Ni^{II} octahedral or six-coordinate complexes generally show very small ZFS owing to higher energy separation between the ground electronic state with the excited state (i.e., 3A_2 to 3T_2). It was shown by us and others that octahedral or pseudo-octahedral complexes would show small ZFS ranging from -10 cm^{-1} to $+10\text{ cm}^{-1}$ and pre-

dicted that in trigonal bipyramidal (TBP) and pentagonal bipyramidal (PBP) geometry Ni^{II} high-spin complexes would display very large magnetic anisotropy.^[13,66]

The heptacoordinate pentagonal bipyramidal Ni^{II} system is expected to yield a negative D value as the $d_{x^2-y^2}$ to d_{xy} orbitals have the same M_L level and the smaller gap between these two orbitals yields a lower energy electronic transition, which can dominantly contribute to the negative D value. We mention first a PBP Ni^{II} complex that was studied by Ruamps et al., that is, $[\text{Ni}(\text{H}_2\text{DAPBH})(\text{H}_2\text{O})_2]\text{NO}_3$ complex (**67**) ($\text{H}_2\text{DAPBH} = 2,6\text{-diacetylpyridine bis}(\text{benzoyl hydrazine})$) where a negative D value of -16.8 cm^{-1} was obtained from NEVPT2 calculations (see Table 2). These values nicely agreed with -12.6 cm^{-1} and -13.9 cm^{-1} extracted from HF-EPR and dc magnetometric measurements.^[18] Recently, Gogoi and co-workers also reported three PBP Ni^{II} complexes, of which $[\text{Ni}(\text{L})(\text{imidazole})_2](\text{NO}_3)_2$ (where $\text{L} = 2,6\text{-diacetylpyridine bishydrazone}$) complex (**68**) was found to possess an axial ZFS of -28.2 cm^{-1} from dc data fitting and -43.5 cm^{-1} from NEVPT2 calculations.^[67] However, ac data is not available for this complex. Boca and co-workers reported a mononuclear octahedral Ni^{II} complex $[\text{Ni}(\text{pydm})_2](\text{dnbz})_2$ (**69**) ($\text{pydm} = 2,6\text{-pyridinedimethanol}$ and $\text{dnbz} = 3,5\text{-dinitrobenzoato}$), which exhibited a negative D parameter of -14.7 cm^{-1} from NEVPT2 calculations (-15.4 cm^{-1} from dc data fit).^[68] Many hepta- or six-coordinate Ni^{II} complexes show small negative ZFS values, which are often not high enough to observe the spin-reversal barrier.

The first giant axial magnetic anisotropy in a Ni TBP complex $[\text{Ni}(\text{Me}_6\text{tren})\text{Cl}]$ (**70**) was reported by Ruamps et al. in 2013 with a calculated D value of -200 cm^{-1} from CASPT2 methodology (see Table 2).^[8] Even high-field high-frequency EPR (HF-EPR) fails to determine the D value directly as the energy separation between the $\pm 1 M_S$ states and 0 state falls beyond the HF-EPR limit. Thus, theoretical calculations are inevitable in such cases. Immediately after this report, Ruiz and co-workers reported a trigonal pyramidal Ni^{II} complex $\text{K}\{\text{Ni}(\text{N}[\text{CH}_2\text{C}(\text{O})\text{NC}(\text{CH}_3)_3]_3)\}$ (**71**), which shows a similar large ZFS value of -200 cm^{-1} estimated from magnetisation measurements and -244 cm^{-1} from the CASPT2-RASSI method.^[69] The reason behind the observation of such large axial ZFS stems from the very closely lying first excited state, which is a consequence of D_3 symmetry and d^8 electronic configuration.^[8,69] The electronic configuration of this type complexes is $d_{xz}^2 d_{yz}^2 d_{x^2-y^2}^2 d_{xy}^1 d_{z^2}^1$ and the near electronic degeneracy between the same M_L levels (± 2) leads to a large magnetic anisotropy. However, the first-order SOC is destroyed by Jahn–Teller (JT) distortion (see Figure 14 b). Therefore, one needs to design and synthesise the ligand environment to fine-tune the ligand field effect and to minimise the Jahn–Teller distortion to obtain a large negative D value. Theoretical analysis revealed that this kind of JT effect could be minimized if we try to constrain the equatorial ligand-metal-ligand bond angles close to 120° , which is the ideal angle in perfect D_{3h} symmetry (see Figure 14 c). Indeed, an optimal ligand environment around the Ni^{II} ion such as DABCO (1,4-diazabicyclo[2.2.2]octane) ligands in the axial position and three halides in the equatorial plane were found to show the highest negative D value known to date for a mono-

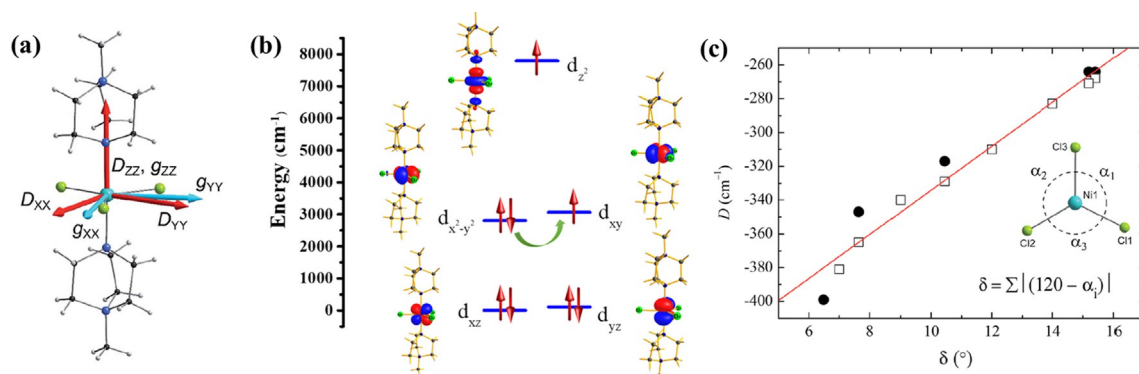


Figure 14. (a) X-ray structure of complex **73** along with computed D , g tensor directions. (b) NEVPT2-LFT computed d orbital splitting diagram of the same. (c) Magneto-structural correlation developed for the δ parameter against computed D values. The black circles are the calculated D values obtained for the X-ray structures collected at high pressure, and the red line is a linear fit. The white squares represent the NEVPT2 computed D values, obtained by altering the δ value of the X-ray structure at ambient pressure.

nuclear Ni^{II} complex, [Ni(MeDABCO)₂Cl₃](ClO₄) (**72**) (see Figure 14a).^[12a,b,70] Although HF-EPR measurements indirectly estimated the D value in the range -400 cm^{-1} to 535 cm^{-1} , ab initio calculations performed later on the same complex confirmed a large D of -400 cm^{-1} . Later, Dunbar and co-workers also reported a trigonal pyramidal Ni^{II} complex ((Me₄N)[Ni(MST)] (**73**), where the D value appears to be a huge -430 cm^{-1} .^[71] However, none of the complexes exhibit a zero-field SIM behaviour despite possessing a very large negative D value, and this is due to a small but non-negligible E value or rhombic splitting parameter present in these complexes. Nevertheless, it was realised that maintaining the D_{3h} symmetry is the key to obtaining such large negative D values in Ni^{II} complexes. A correlation between the coordination number, geometry and the computed D values for the discussed Ni^{II} complexes have been diagrammatically represented in Figure 15 and Figure 16.

Summary and Outlook

To this end, here we have discussed 73 mononuclear first-row late transition-metal complexes, of which 54 complexes are based on the Co^{II} ion and 12 complexes are Fe^{II}, and 7 contain Ni^{II} ions, where detailed theoretical and experimental magnetic studies have been reported. For Co^{II} complexes, the variation in the coordination environment and their corresponding d orbital splitting patterns reveal that a large negative D can be expected for linear ($D_{\infty h}$ or $C_{\infty v}$) geometries, D_{2d} (or elongated tetrahedron) geometries, six-coordinated trigonal (TAP or TP) geometries and in eight-coordinate square anti-prismatic geometries. At the same time, positive D values are anticipated in four-coordinated C_{2v} distorted octahedral and PBP geometries. The most perplexing geometry can be found in five-coordinated complexes, where the fine-tuning of the sign of D is a challenging task. Except for seven coordination, in all of the coordi-

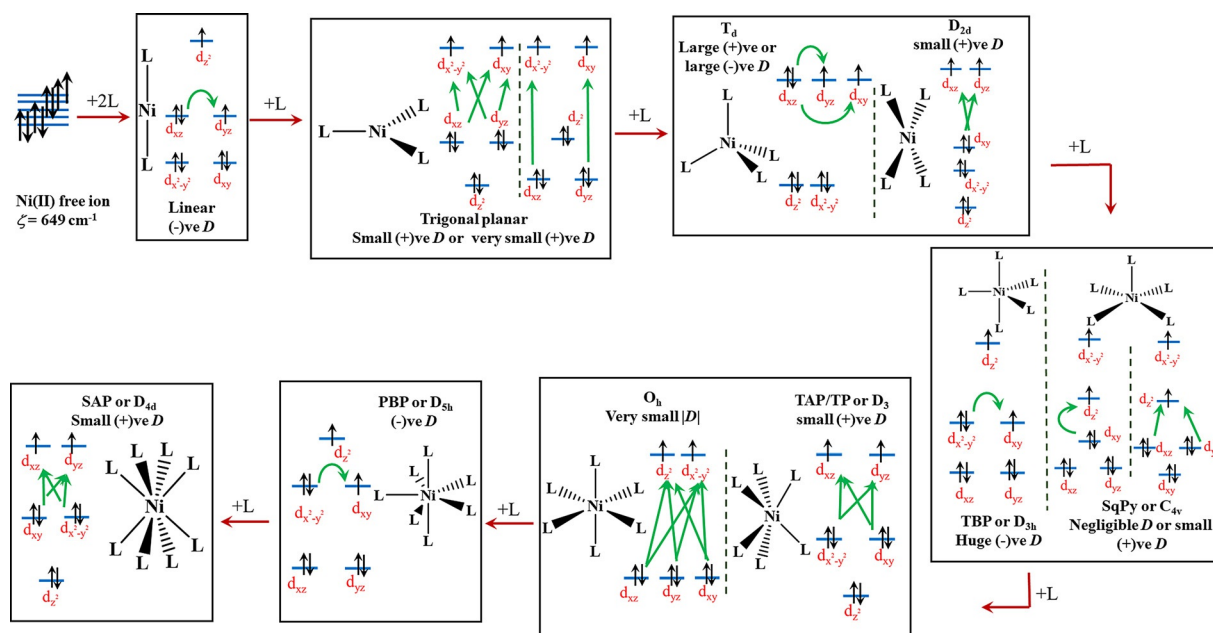


Figure 15. Schematic representation of the successive addition of ligands and their respective change in the qualitative d orbital splitting pattern along with the prediction of D values in the Ni^{II} system. The green arrows indicate the lower energy electronic transitions responsible for ZFS.

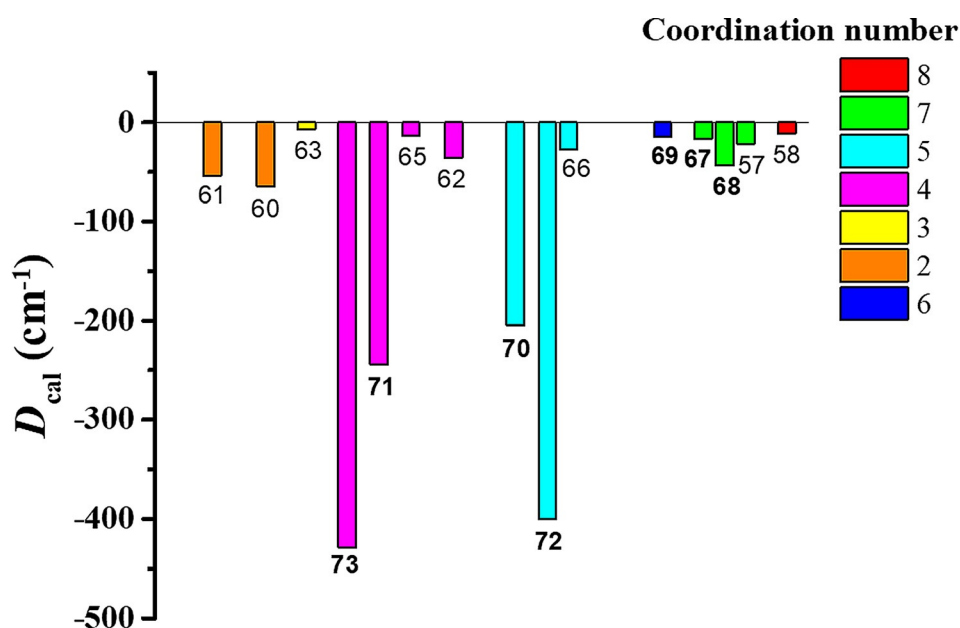


Figure 16. Bar diagram representation of variation of D_{cal} values of selected Fe^{II} and Ni^{II} complexes with respect to different coordination numbers (complex number written below the bars, bold indicates for Ni^{II}). In some of the cases, experimental D is considered when calculated values are not available. In two-coordinate cases, the D values are estimated from $U_{\text{cal}}=3|D|$ for Fe^{II}.

nation geometries, negative D values can be obtained by fine-tuning the ligand design and symmetry around the coordination environment (see Figure 11). The widest range of D values can be obtained in six-coordinated systems as the range of D_{cal} here lies in the range of -120 cm^{-1} to $+140 \text{ cm}^{-1}$. Widely studied or reported geometries for the Co^{II} ion are four-, five- and six-coordinations as these are easier synthetic targets with smaller amendments to existing ligand architectures and also often yield air-stable molecules, and hence characterisations are rather straightforward. Although three- and two-coordinate Co^{II} complexes are very promising and offer very attractive U_{eff} values, which are only next to the best Dy^{III} SIMs, they are unstable in ambient conditions. They, hence, are not robust enough for device fabrication. Although an alternative solution to this problem by using Co^{II}-EMF has been proposed, at present, these are only theoretical predictions waiting for experimental validation. Undoubtedly, the Co^{II} ion is the uncrowned king in the transition metal series to obtain SIMs as it has inherent ability to diminish tunnelling owing to stabilisation of the Kramers state and charge to metal radius ratio, which offer various possible coordination environments that are often difficult to access for other transition metal ions.

If we compare Fe^{II} and Ni^{II} complexes, Fe^{II} shows a larger barrier height (U_{eff}) for two reasons: firstly, the DS_z^2 value for $S=2$ is $4D$ compared with D in the $S=1$ system, and secondly, the probability of quantum tunnelling decreases as the S value increases and therefore it is less severe in $\pm 2 M_S$ levels for $S=2$ compared with $\pm 1 M_S$ levels in $S=1$ (see Figure 16). Unlike the Co^{II} ion, positive D values in Fe^{II} or Ni^{II} complexes never show any spin-reversal barrier as it stabilises the non-magnetic ground state. Both Fe^{II} and Ni^{II} complexes residing in pentagonal bipyramidal, trigonal pyramidal and trigonal bipyramidal

geometry are popular as these geometries exhibit large magnetic anisotropy or U_{eff} . Also, intermediate-spin $S=3/2$ Fe^{II} complexes are better than high-spin Fe^{II} or Ni^{II} complexes, as the anisotropy in these cases is generally larger with QTM being smaller owing to the Kramers nature of the ground state. Possible geometries for various coordination numbers have also been drawn for Fe^{II} and Ni^{II} ions (see Figure 13–Figure 15), where the magnitude as well as sign of D is predicted. In tetrahedral Ni^{II} complexes, high negative or positive D values are predicted, and this has been experimentally verified.^[72]

This review helps to locate the best match between coordination number, geometry and the electronic configuration of the metal ion that yields large negative D values in Fe^{II}, Co^{II} and Ni^{II} mononuclear complexes and consequently helps to understand how very high U_{eff} values can be reached. There are still numerous challenges in this area for both experimentalist and theoreticians, while experimentalists aim to enhance the magnetic anisotropy and diminish rhombic anisotropy by ligand design, it is imperative for the theoretical chemist to explore various avenues in the relaxation mechanism that are not purely controlled by single molecules. Particularly, the effect of lattice vibrations, molecular vibrations, molecular conformations, molecular chirality, hyperfine splitting of Co^{II} ion/coordinated ligand atoms and intermolecular interactions on the magnetisation reversal have been scarcely explored. In this regard, theoretical investigations are crucial to understand other avenues of research in the field of molecular magnetism and to give some fruitful insights. Detailed studies on the spin dynamics, computation of relaxation time, calculation of vibrational degrees of freedom with spin-phonon coupling coefficients are the cutting-edge developments in this area, which

are essential to design room-temperature molecular magnets in the years to come.^[73] This is undoubtedly the need of the hour to keep transition metal ions in the race for the design and development of high-blocking temperature transition metal-based SIMs.

Acknowledgements

G.R. would like to thank DST and SERB (CRG/2018/000430; DST/SJF/CSA-03/2018-10; SB/SJF/2019-20/12) for funding. A.S. and S.D. would like to acknowledge CSIR and UGC, respectively, for the SRF fellowship.

Conflict of interest

The authors declare no conflict of interest.

Keywords: coordination number · geometry · magnetic anisotropy · single-ion magnets · CASSCF

- [1] a) R. P. Feynman, *J. Microelectromech. Syst.* **1992**, *1*, 60–66; b) D. Gatteschi, R. Sessoli, J. Villain, *Molecular Nanomagnets*, Vol. 5, Oxford University Press on Demand, Oxford, **2006**.
- [2] a) C. A. P. Goodwin, F. Ortu, D. Reta, N. F. Chilton, D. P. Mills, *Nature* **2017**, *548*, 439–442; b) F. S. Guo, B. M. Day, Y. C. Chen, M. L. Tong, A. Mansikkamäki, R. A. Layfield, *Angew. Chem. Int. Ed.* **2017**, *56*, 11445–11449; *Angew. Chem.* **2017**, *129*, 11603–11607; c) F.-S. Guo, B. M. Day, Y.-C. Chen, M.-L. Tong, A. Mansikkamäki, R. A. Layfield, *Science* **2018**, *362*, 1400–1403.
- [3] a) M. Mannini, F. Pineider, C. Danieli, F. Totti, L. Sorace, P. Saintavitt, M.-A. Arrio, E. Otero, L. Joly, J. C. Cezar, *Nature* **2010**, *468*, 417–421; b) M. Mannini, F. Pineider, P. Saintavitt, C. Danieli, E. Otero, C. Sciancalepore, A. M. Talarico, M.-A. Arrio, A. Cornia, D. Gatteschi, *Nat. Mater.* **2009**, *8*, 194–197.
- [4] a) P. C. Bunting, M. Atanasov, E. Damgaard-Møller, M. Perfetti, I. Crassee, M. Orlita, J. Overgaard, J. Van Slageren, F. Neese, J. R. Long, *Science* **2018**, *362*, eaat7319; b) X. N. Yao, J. Z. Du, Y. Q. Zhang, X. B. Leng, M. W. Yang, S. D. Jiang, Z. X. Wang, Z. W. Ouyang, L. Deng, B. W. Wang, S. Gao, *J. Am. Chem. Soc.* **2017**, *139*, 373–380.
- [5] a) G. A. Craig, M. Murrie, *Chem. Soc. Rev.* **2015**, *44*, 2135–2147; b) J. M. Frost, K. L. M. Harriman, M. Murugesu, *Chem. Sci.* **2016**, *7*, 2470–2491.
- [6] a) F. Neese, D. A. Pantazis, *Faraday Discuss.* **2011**, *148*, 229–238; b) E. Ruiz, J. Cirera, J. Cano, S. Alvarez, C. Loose, J. Kortus, *Chem. Commun.* **2008**, 52–54; c) O. Waldmann, *Inorg. Chem.* **2007**, *46*, 10035–10037.
- [7] J. Krzystek, J. Telsler, *Dalton Trans.* **2016**, *45*, 16751–16763.
- [8] R. Ruamps, R. Maurice, L. Batchelor, M. Boggio-Pasqua, R. Guillot, A. L. Barra, J. Liu, E. Bendeifel, S. Pillet, S. Hill, T. Mallah, N. Guihery, *J. Am. Chem. Soc.* **2013**, *135*, 3017–3026.
- [9] a) D. Maganas, S. Sottini, P. Kyritsis, E. J. Groenen, F. Neese, *Inorg. Chem.* **2011**, *50*, 8741–8754.
- [10] a) F. Neese, E. I. Solomon, *Magnetism: Molecules to Materials IV: Nano-sized Magnetic Materials*, Wiley-VCH, Weinheim, **2001**, pp. 345–466; b) D. Schweinfurth, M. G. Sommer, M. Atanasov, S. Demeshko, S. Hohloch, F. Meyer, F. Neese, B. Sarkar, *J. Am. Chem. Soc.* **2015**, *137*, 1993–2005; c) D. Schweinfurth, J. Krzystek, M. Atanasov, J. Klein, S. Hohloch, J. Telsler, S. Demeshko, F. Meyer, F. Neese, B. Sarkar, *Inorg. Chem.* **2017**, *56*, 5253–5265; d) F. Neese, *J. Am. Chem. Soc.* **2006**, *128*, 10213–10222; e) F. Neese, E. I. Solomon, *Inorg. Chem.* **1998**, *37*, 6568–6582.
- [11] R. Maurice, R. Bastardis, C. D. Graaf, N. Suaud, T. Mallah, N. Guihery, *J. Chem. Theory Comput.* **2009**, *5*, 2977–2984.
- [12] a) G. A. Craig, A. Sarkar, C. H. Woodall, M. A. Hay, K. E. R. Marriott, K. V. Kamenev, S. A. Moggach, E. K. Brechin, S. Parsons, G. Rajaraman, M. Murrie, *Chem. Sci.* **2018**, *9*, 1551–1559; b) M. Gruden-Pavlović, M. Perić, M. Zlatar, P. García-Fernández, *Chem. Sci.* **2014**, *5*, 1453–1462; c) A. Sarkar, S. Tewary, S. Sinkar, G. Rajaraman, *Chem. Asian J.* **2019**, *14*, 4696–4704; d) G. A. Craig, G. Velmurugan, C. Wilson, R. Valiente, G. Rajaraman, M. Murrie, *Inorg. Chem.* **2019**, *58*, 13815–13825; e) K. R. Vignesh, R. B. Martin, G. Miller, G. Rajaraman, K. S. Murray, S. K. Langley, *Polyhedron* **2019**, *170*, 508–514; f) T. Rajeshkumar, R. Jose, P. R. Remya, G. Rajaraman, *Inorg. Chem.* **2019**, *58*, 11927–11940; g) M. A. Hay, A. Sarkar, K. E. Marriott, C. Wilson, G. Rajaraman, M. Murrie, *Dalton Trans.* **2019**, *48*, 15480–15486; h) Y. Peng, M. K. Singh, V. Mereacre, C. E. Anson, G. Rajaraman, A. K. Powell, *Chem. Sci.* **2019**, *10*, 5528–5538; i) M. K. Singh, G. Rajaraman, *Inorg. Chem.* **2019**, *58*, 3175–3188; j) K. R. Vignesh, S. K. Langley, C. J. Gartshore, I. Borilović, C. M. Forsyth, G. Rajaraman, K. S. Murray, *Dalton Trans.* **2018**, *47*, 11820–11833; k) B. Pandey, K. Ray, G. Rajaraman, *Z. Anorg. Allg. Chem.* **2018**, *644*, 790–800; l) K. R. Vignesh, S. K. Langley, C. J. Gartshore, B. Moubaraki, K. S. Murray, G. Rajaraman, *Inorg. Chem.* **2017**, *56*, 1932–1949; m) T. Gupta, G. Rajaraman, *Chem. Commun.* **2016**, 52, 8972–9008; n) S. K. Singh, K. R. Vignesh, V. Archana, G. Rajaraman, *Dalton Trans.* **2016**, *45*, 8201–8214; o) S. K. Singh, G. Rajaraman, *Nat. Commun.* **2016**, *7*, 10669; p) S. K. Singh, G. Rajaraman, *Chem. Eur. J.* **2014**, *20*, 5214–5218.
- [13] S. Gomez-Coca, E. Cremades, N. Aliaga-Alcalde, E. Ruiz, *J. Am. Chem. Soc.* **2013**, *135*, 7010–7018.
- [14] M. Atanasov, D. Aravena, E. Suturina, E. Bill, D. Maganas, F. Neese, *Coord. Chem. Rev.* **2015**, *289*, 177–214.
- [15] J. Vallejo, I. Castro, R. Ruiz-García, J. Cano, M. Julve, F. Lloret, G. De Munno, W. Wernsdorfer, E. Pardo, *J. Am. Chem. Soc.* **2012**, *134*, 15704–15707.
- [16] S. Tripathi, A. Dey, M. Shanmugam, R. S. Narayanan, V. Chandrasekhar, in *Organometallic Magnets* (Eds.: V. Chandrasekhar, F. Pointillart), Springer, Amsterdam, **2018**, pp. 35–75.
- [17] a) L. Chen, S.-Y. Chen, Y.-C. Sun, Y.-M. Guo, L. Yu, X.-T. Chen, Z. Wang, Z. Ouyang, Y. Song, Z.-L. Xue, *Dalton Trans.* **2015**, *44*, 11482–11490; b) E. Bartolomé, P. J. Alonso, A. Arauzo, J. Luzón, J. Bartolomé, C. Racles, C. Turta, *Dalton Trans.* **2012**, *41*, 10382–10389.
- [18] R. Ruamps, L. J. Batchelor, R. Maurice, N. Gogoi, P. Jiménez-Lozano, N. Guihery, C. de Graaf, A. L. Barra, J. P. Sutter, T. Mallah, *Chem. Eur. J.* **2013**, *19*, 950–956.
- [19] A. K. Mondal, A. Mondal, B. Dey, S. Konar, *Inorg. Chem.* **2018**, *57*, 9999–10008.
- [20] D. Darmanović, I. N. Shcherbakov, C. Duboc, V. Spasojević, D. Hanžel, K. Andelković, D. Radanović, I. Turel, M. Milenković, M. Gruden, B. Čobeljić, M. Zlatar, *J. Phys. Chem. C* **2019**, *123*, 31142–31155.
- [21] B. Drahoš, R. Herchel, Z. Travnicek, *Inorg. Chem.* **2015**, *54*, 3352–3369.
- [22] S.-Q. Su, S.-Q. Wu, M. L. Baker, P. Bencok, N. Azuma, Y. Miyazaki, M. Nakano, S. Kang, Y. Shiota, K. Yoshizawa, *J. Am. Chem. Soc.* **2020**, *142*, 11434–11441.
- [23] a) L. Chen, J. Wang, J. M. Wei, W. Wernsdorfer, X. T. Chen, Y. Q. Zhang, Y. Song, Z. L. Xue, *J. Am. Chem. Soc.* **2014**, *136*, 12213–12216; b) J. M. Wei, Y. Q. Zhang, *Inorg. Chem.* **2015**, *54*, 1203–1205; c) X. X. Jin, X. X. Chen, J. Xiang, Y. Z. Chen, L. H. Jia, B. W. Wang, S. C. Cheng, X. Zhou, C. F. Leung, S. Gao, *Inorg. Chem.* **2018**, *57*, 3761–3774.
- [24] a) Y. Peng, V. Mereacre, C. E. Anson, Y. Zhang, T. Bodenstern, K. Fink, A. K. Powell, *Inorg. Chem.* **2017**, *56*, 6056–6066; b) L. Rigamonti, N. Bridonneau, G. Poneti, L. Tesi, L. Sorace, D. Pinkowicz, J. Jover, E. Ruiz, R. Sessoli, A. Cornia, *Chem. Eur. J.* **2018**, *24*, 8857–8868; c) V. Chandrasekhar, A. Dey, A. J. Mota, E. Colacio, *Inorg. Chem.* **2013**, *52*, 4554–4561.
- [25] a) S. Gómez-Coca, A. Urtizberea, E. Cremades, P. J. Alonso, A. Camon, E. Ruiz, F. Luis, *Nat. Commun.* **2014**, *5*, 4300; b) D. Aravena, D. Venegas-Yazigi, E. Ruiz, *Inorg. Chem.* **2016**, *55*, 6405–6413; c) A. V. Pali, D. V. Korchagin, E. A. Yureva, A. V. Akimov, E. Y. Mischokko, G. V. Shilov, A. D. Talantsev, R. B. Morgunov, S. M. Aldoshin, B. S. Tsukerblat, *Inorg. Chem.* **2016**, *55*, 9696–9706; d) S. Mandal, S. Mondal, C. Rajnak, J. Titis, R. Boca, S. Mohanta, *Dalton Trans.* **2017**, *46*, 13135–13144; e) M. A. Palacios, J. Nehrkorner, E. A. Suturina, E. Ruiz, S. Gomez-Coca, K. Holldack, A. Schnegg, J. Krzystek, J. M. Moreno, E. Colacio, *Chem. Eur. J.* **2017**, *23*, 11649–11661; f) C. Rajnak, F. Varga, J. Titis, J. Moncol, R. Boca, *Inorg. Chem.* **2018**, *57*, 4352–4358; g) D. Sertphon, K. S. Murray, W. Phonsri, J. Jover, E. Ruiz, S. G. Telfer, A. Alkas, P. Harding, D. J. Harding, *Dalton Trans.* **2018**, *47*, 859–867; h) J. Acharya, A. Swain, A. Chakraborty, V. Kumar, P. Kumar, J. F. Gonzalez, O. Cador, F. Pointillart, G. Rajaraman, V. Chandrasekhar, *Inorg. Chem.* **2019**, *58*, 10725–10735.

- [26] Y.-F. Deng, M. K. Singh, D. Gan, T. Xiao, Y. Wang, S. Liu, Z. Wang, Z. Ouyang, Y.-Z. Zhang, K. R. Dunbar, *Inorg. Chem.* **2020**, *59*, 7622–7630.
- [27] M. R. Saber, M. K. Singh, K. R. Dunbar, *Chem. Commun.* **2020**, *56*, 8492–8495.
- [28] D. H. Moseley, S. E. Stavretis, K. Thirunavukkuarasu, M. Ozerov, Y. Cheng, L. L. Daemen, J. Ludwig, Z. Lu, D. Smirnov, C. M. Brown, A. Pandey, A. J. Ramirez-Cuesta, A. C. Lamb, M. Atanasov, E. Bill, F. Neese, Z. L. Xue, *Nat. Commun.* **2018**, *9*, 2572.
- [29] a) Y.-Y. Zhu, C. Cui, Y.-Q. Zhang, J.-H. Jia, X. Guo, C. Gao, K. Qian, S.-D. Jiang, B.-W. Wang, Z.-M. Wang, S. Gao, *Chem. Sci.* **2013**, *4*, 1802–1806; b) V. V. Novikov, A. A. Pavlov, Y. V. Nelyubina, M. E. Boulon, O. A. Varzatskii, Y. Z. Voloshin, R. E. Winpenny, *J. Am. Chem. Soc.* **2015**, *137*, 9792–9795; c) Y. Y. Zhu, Y. Q. Zhang, T. T. Yin, C. Gao, B. W. Wang, S. Gao, *Inorg. Chem.* **2015**, *54*, 5475–5486; d) A. A. Pavlov, Y. V. Nelyubina, S. V. Kats, L. V. Penkova, N. N. Efimov, A. O. Dmitrienko, A. V. Vologzhanina, A. S. Belov, Y. Z. Voloshin, V. V. Novikov, *J. Phys. Chem. Lett.* **2016**, *7*, 4111–4116; e) Y. Peng, T. Bodenstern, K. Fink, V. Mereacre, C. E. Anson, A. K. Powell, *Phys. Chem. Chem. Phys.* **2016**, *18*, 30135–30143; f) Y. Z. Zhang, S. Gomez-Coca, A. J. Brown, M. R. Saber, X. Zhang, K. R. Dunbar, *Chem. Sci.* **2016**, *7*, 6519–6527; g) T. J. Ozumerzifon, I. Bhowmick, W. C. Spaller, A. K. Rappe, M. P. Shores, *Chem. Commun.* **2017**, *53*, 4211–4214.
- [30] a) M. Pinsky, D. Avnir, *Inorg. Chem.* **1998**, *37*, 5575–5582; b) S. Alvarez, D. Avnir, M. Lluell, M. Pinsky, *New J. Chem.* **2002**, *26*, 996–1009.
- [31] B. Yao, M. K. Singh, Y. F. Deng, Y. N. Wang, K. R. Dunbar, Y. Z. Zhang, *Inorg. Chem.* **2020**, *59*, 8505–8513.
- [32] a) M. A. Hay, A. Sarkar, G. A. Craig, L. Bhaskaran, J. Nehrkorner, M. Ozerov, K. E. R. Marriott, C. Wilson, G. Rajaraman, S. Hill, M. Murrie, *Chem. Sci.* **2019**, *10*, 6354–6361; b) J. Acharya, A. Sarkar, P. Kumar, V. Kumar, J. F. Gonzalez, O. Cador, F. Pointillart, G. Rajaraman, V. Chandrasekhar, *Dalton Trans.* **2020**, *49*, 4785–4796.
- [33] a) X. Hou, X. Wang, X. Liu, J. Wang, L. Tang, P. Ju, *New J. Chem.* **2018**, *42*, 8583–8590; b) C. Rajnák, J. Titiš, I. Šalitroš, R. Boča, O. Fuhr, M. Ruben, *Polyhedron* **2013**, *65*, 122–128; c) R. Boča, L. U. Dlhán, W. Linert, H. Ehrenberg, H. Fuess, W. Haase, *Chem. Phys. Lett.* **1999**, *307*, 359–366; d) A. K. Mondal, J. Jover, E. Ruiz, S. Konar, *Chem. Commun.* **2017**, *53*, 5338–5341.
- [34] T. Jurca, A. Farghal, P. H. Lin, I. Korobkov, M. Murugesu, D. S. Richeson, *J. Am. Chem. Soc.* **2011**, *133*, 15814–15817.
- [35] F. Shao, B. Cahier, E. Rivière, R. Guillot, N. Guihéry, V. E. Campbell, T. Mallah, *Inorg. Chem.* **2017**, *56*, 1104–1111.
- [36] a) F. Shao, B. Cahier, Y. T. Wang, F. L. Yang, E. Rivière, R. Guillot, N. Guihéry, J. P. Tong, T. Mallah, *Chem. Asian J.* **2020**, *15*, 391–397; b) R. Ruamps, L. J. Batchelor, R. Guillot, G. Zakhia, A.-L. Barra, W. Wernsdorfer, N. Guihéry, T. Mallah, *Chem. Sci.* **2014**, *5*, 3418–3424; c) B. Cahier, M. Perfetti, G. Zakhia, D. Naoufal, F. El-Khatib, R. Guillot, E. Rivière, R. Sessoli, A. L. Barra, N. Guihéry, *Chem. Eur. J.* **2017**, *23*, 3648–3657; d) B. Cahier, R. Maurice, H. Bolvin, T. Mallah, N. Guihéry, *Magnetochem.* **2016**, *2*, 31.
- [37] J. M. Zadrozny, J. R. Long, *J. Am. Chem. Soc.* **2011**, *133*, 20732–20734.
- [38] K. Fukui, N. Kojima, H. Ohya-Nishiguchi, N. Hirota, *Inorg. Chem.* **1992**, *31*, 1338–1344.
- [39] a) M. S. Fataftah, S. C. Coste, B. Vlasisavljevich, J. M. Zadrozny, D. E. Freedman, *Chem. Sci.* **2016**, *7*, 6160–6166; b) E. A. Sutorina, D. Maganas, E. Bill, M. Atanasov, F. Neese, *Inorg. Chem.* **2015**, *54*, 9948–9961; c) S. Vaidya, S. Tewary, S. K. Singh, S. K. Langley, K. S. Murray, Y. Lan, W. Wernsdorfer, G. Rajaraman, M. Shanmugam, *Inorg. Chem.* **2016**, *55*, 9564–9578; d) E. A. Sutorina, J. Nehrkorner, J. M. Zadrozny, J. Liu, M. Atanasov, T. Weyhermuller, D. Maganas, S. Hill, A. Schnegg, E. Bill, J. R. Long, F. Neese, *Inorg. Chem.* **2017**, *56*, 3102–3118; e) K. Chattopadhyay, M. A. J. Heras Ojea, A. Sarkar, M. Murrie, G. Rajaraman, D. Ray, *Inorg. Chem.* **2018**, *57*, 13176–13187.
- [40] a) S. Vaidya, A. Upadhyay, S. K. Singh, T. Gupta, S. Tewary, S. K. Langley, J. P. Walsh, K. S. Murray, G. Rajaraman, M. Shanmugam, *Chem. Commun.* **2015**, *51*, 3739–3742; b) A. K. Mondal, M. Sundararajan, S. Konar, *Dalton Trans.* **2018**, *47*, 3745–3754; c) S. Vaidya, P. Shukla, S. Tripathi, E. Riviere, T. Mallah, G. Rajaraman, M. Shanmugam, *Inorg. Chem.* **2018**, *57*, 3371–3386.
- [41] S. Vaidya, S. K. Singh, P. Shukla, K. Ansari, G. Rajaraman, M. Shanmugam, *Chem. Eur. J.* **2017**, *23*, 9546–9559.
- [42] S. Tripathi, S. Vaidya, K. U. Ansari, N. Ahmed, E. Riviere, L. Spillecke, C. Koo, R. Klingeler, T. Mallah, G. Rajaraman, M. Shanmugam, *Inorg. Chem.* **2019**, *58*, 9085–9100.
- [43] a) M. S. Fataftah, J. M. Zadrozny, D. M. Rogers, D. E. Freedman, *Inorg. Chem.* **2014**, *53*, 10716–10721.
- [44] Y. Rechkemmer, F. D. Breitgoff, M. van der Meer, M. Atanasov, M. Haki, M. Orlita, P. Neugebauer, F. Neese, B. Sarkar, J. van Slageren, *Nat. Commun.* **2016**, *7*, 10467.
- [45] A. Eichhöfer, Y. Lan, V. Mereacre, T. Bodenstern, F. Weigend, *Inorg. Chem.* **2014**, *53*, 1962–1974.
- [46] Y. F. Deng, Z. Wang, Z. W. Ouyang, B. Yin, Z. Zheng, Y. Z. Zheng, *Chem. Eur. J.* **2016**, *22*, 14821–14825.
- [47] Y.-F. Deng, T. Han, B. Yin, Y.-Z. Zheng, *Inorg. Chem. Front.* **2017**, *4*, 1141–1148.
- [48] J. M. Zadrozny, D. J. Xiao, M. Atanasov, G. J. Long, F. Grandjean, F. Neese, J. R. Long, *Nat. Chem.* **2013**, *5*, 577–581.
- [49] M. K. Singh, N. Yadav, G. Rajaraman, *Chem. Commun.* **2015**, *51*, 17732–17735.
- [50] M. K. Singh, P. Shukla, M. Khatua, G. Rajaraman, *Chem. Eur. J.* **2020**, *26*, 464–477.
- [51] a) S. Mossin, B. L. Tran, D. Adhikari, M. Pink, F. W. Heinemann, J. Sutter, R. K. Szilagy, K. Meyer, D. J. Mindiola, *J. Am. Chem. Soc.* **2012**, *134*, 13651–13661; b) X. Feng, S. J. Hwang, J. L. Liu, Y. C. Chen, M. L. Tong, D. G. Nocera, *J. Am. Chem. Soc.* **2017**, *139*, 16474–16477.
- [52] S. Roy Chowdhury, S. Mishra, *J. Chem. Phys.* **2018**, *149*, 234302.
- [53] A. Sarkar, G. Velmurugan, T. Rajeshkumar, G. Rajaraman, *Dalton Trans.* **2018**, *47*, 9980–9984.
- [54] A. K. Bar, C. Pichon, N. Gogoi, C. Duhayon, S. Ramasesha, J. P. Sutter, *Chem. Commun.* **2015**, *51*, 3616–3619.
- [55] A. K. Bar, N. Gogoi, C. Pichon, V. M. Goli, M. Thlijeni, C. Duhayon, N. Suaud, N. Guihery, A. L. Barra, S. Ramasesha, J. P. Sutter, *Chem. Eur. J.* **2017**, *23*, 4380–4396.
- [56] J. Xiang, J. J. Liu, X. X. Chen, L. H. Jia, F. Yu, B. W. Wang, S. Gao, T. C. Lau, *Chem. Commun.* **2017**, *53*, 1474–1477.
- [57] a) W. M. Reiff, A. M. LaPointe, E. H. Witten, *J. Am. Chem. Soc.* **2004**, *126*, 10206–10207; b) W. M. Reiff, C. E. Schulz, M.-H. Whangbo, J. I. Seo, Y. S. Lee, G. R. Potratz, C. W. Spicer, G. S. Girolami, *J. Am. Chem. Soc.* **2008**, *130*, 404–405; c) W. Alexander Merrill, T. A. Stich, M. Brynda, G. J. Yeagle, J. C. Fettinger, R. D. Hont, W. M. Reiff, C. E. Schulz, R. D. Britt, P. P. Power, *J. Am. Chem. Soc.* **2009**, *131*, 12693–12702.
- [58] a) D. E. Freedman, W. H. Harman, T. D. Harris, G. J. Long, C. J. Chang, J. R. Long, *J. Am. Chem. Soc.* **2010**, *132*, 1224–1225; b) W. H. Harman, T. D. Harris, D. E. Freedman, H. Fong, A. Chang, J. D. Rinehart, A. Ozarowski, M. T. Sougrati, F. Grandjean, G. J. Long, *J. Am. Chem. Soc.* **2010**, *132*, 18115–18126.
- [59] a) M. Atanasov, D. Ganyushin, D. A. Pantazis, K. Sivalingam, F. Neese, *Inorg. Chem.* **2011**, *50*, 7460–7477; b) M. Atanasov, J. M. Zadrozny, J. R. Long, F. Neese, *Chem. Sci.* **2013**, *4*, 139–156; c) J. M. Zadrozny, M. Atanasov, A. M. Bryan, C.-Y. Lin, B. D. Rekker, P. P. Power, F. Neese, J. R. Long, *Chem. Sci.* **2013**, *4*, 125–138.
- [60] A. Lunghi, F. Totti, R. Sessoli, S. Sanvito, *Nat. Commun.* **2017**, *8*, 14620.
- [61] H. Andres, E. L. Bominaar, J. M. Smith, N. A. Eckert, P. L. Holland, E. Münck, *J. Am. Chem. Soc.* **2002**, *124*, 3012–3025.
- [62] P. H. Lin, N. C. Smythe, S. I. Gorelsky, S. Maguire, N. J. Henson, I. Korobkov, B. L. Scott, J. C. Gordon, R. T. Baker, M. Murugesu, *J. Am. Chem. Soc.* **2011**, *133*, 15806–15809.
- [63] J. M. Zadrozny, S. M. Greer, S. Hill, D. E. Freedman, *Chem. Sci.* **2016**, *7*, 416–423.
- [64] C. G. Werncke, M. A. Bouammali, J. Baumard, N. Suaud, C. Martins, N. Guihery, L. Vendier, J. Zheng, J. B. Sortais, C. Darcel, S. Sabo-Etienne, J. P. Sutter, S. Bontemps, C. Pichon, *Inorg. Chem.* **2016**, *55*, 10968–10977.
- [65] M. A. Hay, A. Sarkar, G. A. Craig, K. E. R. Marriott, C. Wilson, G. Rajaraman, M. Murrie, *Chem. Commun.* **2020**, *56*, 6826–6829.
- [66] S. K. Singh, T. Gupta, P. Badkur, G. Rajaraman, *Chem. Eur. J.* **2014**, *20*, 10305–10313.
- [67] M. Dey, P. P. Mudoi, A. Choudhury, B. Sarma, N. Gogoi, *Chem. Commun.* **2019**, *55*, 11547–11550.
- [68] J. Titiš, V. Chrenkova, C. Rajnák, J. Moncol, D. Valigura, R. Boca, *Dalton Trans.* **2019**, *48*, 11647–11650.
- [69] S. Gómez-Coca, E. Cremades, N. Aliaga-Alcalde, E. Ruiz, *Inorg. Chem.* **2014**, *53*, 676–678.
- [70] K. E. R. Marriott, L. Bhaskaran, C. Wilson, M. Medarde, S. T. Ochsenshein, S. Hill, M. Murrie, *Chem. Sci.* **2015**, *6*, 6823–6828.
- [71] K. A. Schulte, K. R. Vignesh, K. R. Dunbar, *Chem. Sci.* **2018**, *9*, 9018–9026.

[72] S. D. Jiang, D. Maganas, N. Levesanos, E. Ferentinos, S. Haas, K. Thirunavukkuarasu, J. Krzystek, M. Dressel, L. Bogani, F. Neese, P. Kyritsis, *J. Am. Chem. Soc.* **2015**, *137*, 12923–12928.

[73] a) A. Lunghi, S. Sanvito, *J. Phys. Chem. Lett.* **2020**, *11*, 6273–6278; b) A. Castro-Alvarez, Y. Gil, L. Llanos, D. Aravena, *Inorg. Chem. Front.* **2020**, *7*, 2478–2486.

Manuscript received: July 7, 2020

Accepted manuscript online: July 30, 2020

Version of record online: October 12, 2020
